The Journal of Chemical Physics

A comprehensive benchmark *ab initio* survey of the stationary points and products of the OH· + CH_3OH system

Cite as: J. Chem. Phys. **158**, 034301 (2023); https://doi.org/10.1063/5.0133978
Submitted: 07 November 2022 • Accepted: 20 December 2022 • Accepted Manuscript Online: 21 December 2022 • Published Online: 17 January 2023

Tibor Győri and Gábor Czakó

The Journal of Chemical Physics ARTICLE scitation.org/journal/jcp

A comprehensive benchmark *ab initio* survey of the stationary points and products of the OH· + CH_3OH system

Cite as: J. Chem. Phys. 158, 034301 (2023); doi: 10.1063/5.0133978
Submitted: 7 November 2022 • Accepted: 20 December 2022 •
Published Online: 17 January 2023

Tibor Győri[a] and Gábor Czakó[a]

AFFILIATIONS

MTA-SZTE Lendület Computational Reaction Dynamics Research Group, Interdisciplinary Excellence Centre and Department of Physical Chemistry and Materials Science, Institute of Chemistry, University of Szeged, Rerrich Béla tér 1, Szeged H-6720, Hungary

[a]**Authors to whom correspondence should be addressed:** tibor.gyori@chem.u-szeged.hu and gczako@chem.u-szeged.hu

ABSTRACT

Reactions between methanol and the hydroxyl radical are of significant interest for combustion-, atmospheric-, and astrochemistry. While the two primary product channels (the formation of H_2O with either CH_3O· or ·CH_2OH) have been the subject of numerous studies, the possibility of other products has seen little attention. Here, we present a comprehensive thermochemical survey of the stationary points and plausible products of the reaction, featuring 29 geometries optimized at the UCCSD(T)-F12b/aug-cc-pVTZ level, followed by accurate composite *ab initio* computations for all stationary points (including ·CH_2OH dissociation and isomerization) and five product channels, with a detailed evaluation of basis set convergence and efficiency. The computations reveal that the formation of methanediol and the hydroxymethoxy radical is thermodynamically favorable and the endothermicity of formaldehyde formation is low enough to be a plausible product channel. We also observe unexpectedly large energy deviations between the partially-spin-adapted ROHF-RCCSD(T) method and ROHF-UCCSD(T) as well as between UHF-UCCSDT(Q) and ROHF-UCCSDT(Q) results.

I. INTRODUCTION

Both methanol (CH_3OH) and the hydroxyl radical (·OH) are important species in their own right in combustion-, atmospheric- and astrochemistry.[1–8]

Methanol plays a role in atmospheric chemistry, as it is present in small amounts in Earth's atmosphere,[9] both directly from industrial and biological sources, and indirectly from the breakdown of more complicated molecules, such as methyl *tert*-butyl ether (MTBE), a common gasoline additive.

As the simplest alcohol and a potential alternative to fossil fuels,[10] its combustion chemistry has been the subject of numerous studies[5,6] and owing to its abundance in interstellar media (ISM) as well as its proposed roles[11] in the formation and breakdown of complex organic molecules in space it has seen considerable attention within astrochemistry.

Likewise, ·OH is also of major interest as it is one of the most important reactive oxidants in combustion and the atmosphere,[4,8] and a key species in ISM.

Considering the above, it is no wonder that a large number of theoretical studies[11–25] have investigated the reaction of methanol and ·OH either as the main topic or incidentally, by discussing one of the possible products,[26–36] often as part of a study focusing on reaction kinetics or spectroscopy.

Perhaps due to the aforementioned focus on the kinetics of ·CH_2OH formation,

$$CH_3OH + \cdot OH = \cdot CH_2OH + H_2O, \quad \text{(R1)}$$

and CH_3O· formation,

$$CH_3OH + \cdot OH = CH_3O\cdot + H_2O, \quad \text{(R2)}$$

a comprehensive high-accuracy survey of the ·OH + CH_3OH system that examines the thermochemistry of all known stationary points and plausible products on an equal footing is yet to be published. The present work aims to remedy that and to serve as a prelude to our full-dimensional global reactive potential energy surface (PES).

We also probe the following questions related to the methodology of computing accurate potential energies for open-shell systems:

- Is the difference in relative energies between standard spin-orbital coupled-cluster methods and a partially spin-restricted coupled cluster method[37] negligible when using a restricted open-shell Hartree–Fock (ROHF) reference?
- Are the cc-pV*n*Z-F12 basis sets sufficiently diffuse for describing noncovalent interactions between a polar radical and a polar closed shell molecule?
- What is the impact of the choice of reference wavefunction type (UHF or ROHF) for calculating high-order coupled-cluster contributions to relative energies in a high-accuracy composite scheme?
- Which basis sets or extrapolation schemes are on the Pareto frontier when it comes to the trade-off between approaching the complete-basis-set (CBS) limit of CCSD(T) and computational cost?

The paper is organized as the following: Sec. II contains details of the quantum chemistry computations, Sec. III presents the results of the geometry optimizations, Sec. IV discusses the results of high-accuracy single-point calculations, and finally Sec. V summarizes the results.

II. COMPUTATIONAL DETAILS

Most computations presented in this work were performed with Molpro 2015.1.44.[38–49] All coupled-cluster (CC) calculations with an unrestricted Hartree–Fock (UHF) reference were performed with the MRCC package[50–55] via the Molpro-MRCC interface. MRCC was used as a standalone program for restricted open-shell Hartree–Fock (ROHF) reference CC calculations beyond CCSD(T). Basis sets not included in Molpro 2015.1.44 were obtained from the MolSSI Basis Set Exchange website.[56–58]

All post-HF calculations in this work make use of a ROHF reference and the frozen-core approximation unless specified otherwise. All relative energies are reported relative to free reactants (·OH + CH_3OH), unless specified otherwise.

We have encountered HF convergence issues at several geometries of this system, and for this reason, we have used the ManyHF method[59] to reliably obtain the lowest energy restricted open-shell Hartree–Fock (ROHF) solution, both during geometry optimizations, as well as single-point calculations. In a nutshell, ManyHF performs multiple HF calculations, starting from different guess orbitals, and the HF solution with the lowest energy is used as the reference for the single-reference post-HF calculations that follow it.

Geometries were initially optimized using restricted open-shell second-order Møller–Plesset perturbation theory (RMP2)[45] and the aug-cc-pVDZ (AVDZ) basis set.[60,61] Initial geometries were either taken from the literature or manually crafted in Avogadro.[62]

The geometries obtained at the RMP2/AVDZ level were then refined using an unrestricted explicitly-correlated CC singles, doubles, and perturbative triples [UCCSD(T)-F12b] method[48] and the aug-cc-pVTZ (AVTZ) basis set.[60,61]

Additionally, to probe the impact of using a spin-unrestricted CC theory, we have also reoptimized the geometries at a partially spin-restricted CC method[37] [RCCSD(T)-F12b] and the AVTZ basis set. All optimizations were converged to tight convergence criteria for energy change, gradient, as well as displacement. To avoid any spurious symmetry enforcement, all optimizations were performed with point-group symmetry disabled.

Harmonic vibrational frequencies were also computed at the RMP2/AVDZ, UCCSD(T)-F12b/AVTZ, and RCCSD(T)-F12b/AVTZ levels. Both gradients and Hessians were obtained numerically during optimizations and frequency calculations. The numerical differentiation parameters were left at their default values, with three caveats:

- Instead of reusing the orbitals of a previous optimization step or displacement, all displacements for numerical gradients performed the entire ManyHF procedure
- For finalizing optimizations, four-point numerical gradients were used for some geometries
- For Hessians, the ManyHF procedure was only performed once, at the geometry for which the Hessian was to be computed

A subset of the final UCCSD(T)-F12b/AVTZ geometries were then used in subsequent single-point computations to yield our benchmark classical (ZPE-exclusive) energies, which were calculated according to Eq. (1),

$$E_{\text{classical}} = E(\text{UCCSD-F12b/aug-cc-pwCV5Z}) + \delta[(\text{T})/\text{CBS}] + \delta[\text{T}] + \delta[(\text{Q})] + \Delta_{\text{core}} + \Delta_{\text{rel}} + \Delta_{\text{SO}}. \quad (1)$$

The starting point for our benchmark energy expression is a UCCSD-F12b calculation using the extremely large aug-cc-pwCV5Z basis set[60,61,63] with the aug-cc-pwCV5Z/MP2fit[64] and aug-cc-pV5Z/JKfit[65,66] auxiliary basis sets and an F12 geminal exponent of $\beta = 1.4$. Using the AwCV5Z basis set instead of AV5Z provides a radial flexibility that even frozen-core valence correlation energies benefit from.

Both the UCCSD-F12b correlation energy and the ROHF energy are used without extrapolation. The F12 complete auxiliary basis set (CABS) correction is included in the HF energy, which is expected to eliminate almost all remaining basis set error from the HF energy when used with large enough basis sets,[67] thus eliminating the need for HF energy extrapolation.

$\delta[(\text{T})/\text{CBS}]$ is calculated as a two-point L^{-3} extrapolation[68,69] [Eq. (2)] from (T) contributions obtained from UCCSD(T)-F12b computations using the cc-pVQZ-F12[70] and cc-pV5Z-F12(rev2)[67] basis sets (abbreviated as VQZ-F12 and V5Z-F12 v2) and $\beta = 1$.

For VQZ-F12 calculations, the default auxiliary basis set choice of Molpro 2015 was used (cc-pVQZ/JKfit,[65] aug-cc-pVQZ/MP2fit,[71] and cc-pVQZ-F12/OptRI[72]). Molpro 2015 has no default auxiliary basis sets for V5Z-F12 v2, thus aug-cc-pwCV5Z/MP2fit and aug-cc-pV5Z/JKfit were used, just like the aug-cc-pwCV5Z calculation *vide supra*. The CBS limit of the (T) term is obtained by the expression

$$\delta[(\text{T})/\text{CBS}] = (\text{T})_{\text{V5Z-F12v2}} + \frac{(\text{T})_{\text{V5Z-F12v2}} - (\text{T})_{\text{VQZ-F12}}}{\left(\frac{5}{4}\right)^3 - 1}. \quad (2)$$

$\delta[\text{T}]$ is calculated as the following:

$$\delta[\mathrm{T}] = E(\mathrm{ROHF\text{-}UCCSDT/AVDZ}) - E(\mathrm{ROHF\text{-}UCCSD(T)/AVDZ}). \quad (3)$$

Likewise, $\delta[(\mathrm{Q})]$ is calculated as the following:

$$\delta[(\mathrm{Q})] = E\left(\mathrm{ROHF\text{-}UCCSDT(Q)}_{/\mathrm{B}}/\mathrm{AVDZ}\right) - E(\mathrm{ROHF\text{-}UCCSDT/AVDZ}). \quad (4)$$

MRCC supports multiple ROHF referenced (Q) methods, and we have chosen $(\mathrm{Q})_{/\mathrm{B}}$ as it appears to be more robust than $(\mathrm{Q})_{/\mathrm{A}}$ without incurring the additional computational cost of $(\mathrm{Q})_{\Lambda}$.[73]

These post-(T) corrections can also be calculated using UHF reference wavefunctions and to probe the effect of the ROHF/UHF choice, we have performed all post-(T) calculations with both.

The core correlation correction Δ_{core} is calculated as the difference of frozen-core (FC) and all-electron (AE) UCCSD(T)-F12b calculations with the cc-pCVQZ-F12 basis set[74] and an F12 geminal exponent of $\beta = 1.5$. The choice of auxiliary basis sets was left at the Molpro 2015 defaults associated with this basis set: aug-cc-pVQZ/JKfit,[65,66] aug-cc-pVQZ/MP2fit,[71] and cc-pVQZ-F12/OptRI,[72]

$$\Delta_{\mathrm{core}} = E(\mathrm{AE\text{-}UCCSD(T)\text{-}F12b/cc\text{-}pCVQZ\text{-}F12}) - E(\mathrm{FC\text{-}UCCSD(T)\text{-}F12b/cc\text{-}pCVQZ\text{-}F12}). \quad (5)$$

The scalar relativistic contribution Δ_{rel} is obtained with the second-order Douglas-Kroll-Hess method,[75] the aug-cc-pwCVTZ basis set[60,61,63] and the corresponding DK-optimized aug-cc-pwCVTZ-DK basis set,[60,61,63,76,77]

$$\Delta_{\mathrm{rel}} = E(\mathrm{DK\text{-}AE\text{-}UCCSD(T)/aug\text{-}cc\text{-}pwCVTZ\text{-}DK}) - E(\mathrm{AE\text{-}UCCSD(T)/aug\text{-}cc\text{-}pwCVTZ}). \quad (6)$$

Finally, a spin–orbit coupling correction (Δ_{SO}) is obtained with the aug-cc-pVQZ (AVQZ) basis set,[60,61] by first performing a two-state, Davidson-corrected[78,79] multireference configuration interaction calculation with single and double excitations[80–82] and an active space of 21 electrons in 11 orbitals, denoted as MRCI+Q(21,11). The MRCI calculation uses a two-state, state-averaged CASSCF(21,11).[41,42] The SO correction is obtained from the MRCI wavefunction with the interacting-states approach,[49] as the difference between the SO ground state (SO_1) and non-SO ground state (non-SO_1) energies,

$$\Delta_{\mathrm{SO}} = \mathrm{SO}_1(\mathrm{MRCI+Q/AVQZ}) - \text{non-}\mathrm{SO}_1(\mathrm{MRCI+Q/AVQZ}). \quad (7)$$

Our benchmark adiabatic energies are calculated as the following:

$$E_{\mathrm{adiabatic}} = \Delta_r H(0\,K) = E_{\mathrm{classical}} + \Delta_{\mathrm{ZPE}}, \quad (8)$$

where Δ_{ZPE} is the vibrational zero-point energy correction, obtained using the harmonic oscillator approximation, at the UCCSD(T)-F12b/AVTZ level.

To probe the basis set convergence of the FC-CCSD(T)-F12b relative energies as well as the HF, CCSD, and (T) contributions additional single-point calculations were performed at the 19 geometries chosen for composite energy calculations (and the free reactants), with the following basis sets:

- AVQZ
- aug-cc-pV5Z (AV5Z)[60,61]
- cc-pVTZ-F12 (VTZ-F12)[70]
- aug-cc-pVTZ-F12 (AVTZ-F12)[83]
- aug-cc-pVQZ-F12 (AVQZ-F12)[83]

To evaluate the impact of basis set extrapolation, we have also calculated TZ/QZ and QZ/5Z CBS extrapolations of the valence CCSD-F12b and (T) correlation energies using a more general form of Eq. (2),

$$E_{\mathrm{CBS}} = \mathrm{E}_{n\mathrm{Z}} + \frac{E_{n\mathrm{Z}} - E_{(n-1)\mathrm{Z}}}{\left(\frac{n}{n-1}\right)^{\alpha} - 1}, \quad (9)$$

where $n = 5$ for QZ/5Z extrapolations, $n = 4$ for TZ/QZ and α is the extrapolation exponent. For the extrapolation of valence CCSD-F12b correlation energy, different basis set pairs were extrapolated with different values of α:

- AV{T,Q}Z used the empirical[84] $\alpha = 4.25$
- AV{Q,5}Z used the empirical[84] $\alpha = 4.9$
- V{T,Q}Z-F12 and AV{T,Q}Z-F12 used the empirical[84] $\alpha = 4.6$
- V{Q,5}Z-F12 used the empirical[85] $\alpha = 6$

To probe the sensitivity of the extrapolation coefficient AV{Q,5}Z, V{T,Q}Z-F12, and AV{T,Q}Z-F12, extrapolations have also been calculated using the theoretically justifiable[86] $\alpha = 7$. All extrapolations of the valence (T) correlation energy use $\alpha = 3$.

Reference data for the 0 K reaction enthalpies of the various product channels were obtained from the ATcT thermochemical network, version 1.122r.[87–89] Both the enthalpies and their uncertainties were obtained via the ATcT website's reaction search functionality, which automatically computes the uncertainty of the reaction enthalpy using the full covariance matrix of the thermochemical network. All ATcT reaction queries used in this work have been archived on the Internet Archive[90] for preservation, hyperlinks to these snapshots are provided in the list of references.

III. RESULTS OF GEOMETRY OPTIMIZATIONS

A. Formation of $CH_3O\cdot$ and $\cdot CH_2OH$

The results of our ROHF-UCCSD(T)-F12b/AVTZ geometry optimizations for the two primary[16] pathways leading to $CH_3O\cdot + H_2O$ and $\cdot CH_2OH + H_2O$ are shown in Fig. 1. Tables of RMP2/AVDZ, UCCSD(T)-F12b/AVTZ, and RCCSD(T)-F12b/AVTZ energies and Cartesian coordinates can be found in the supplementary material.

Our geometries largely match geometries found in the literature, with a few noteworthy exceptions. Previous works have disagreed on the exact geometry and point-group symmetry of the reactant complex minimum (RC1), with Gao *et al.* reporting[16] a C_s symmetric geometry and Nguyen *et al.* reporting[22] a non-symmetric minimum, with a noticeable HCOO dihedral bend of 32.7°.

Our results support the asymmetry of RC1, with an HCOO dihedral angle of 24.7°. Furthermore, we have actually found the C_s symmetric reactant complex geometry to be a first-order

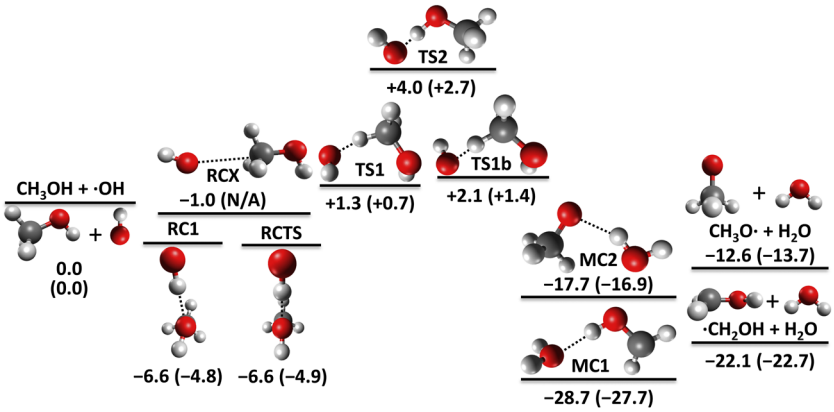

FIG. 1. Relative classical and adiabatic energies of the primary products and stationary points of the CH_3OH + ·OH system at the UCCSD(T)-F12b/AVTZ level. Adiabatic energies are given in parentheses, and all energies are in kcal/mol.

saddle point (RCTS), with a classical energy only 0.010 kcal/mol above the true reactant minimum and an imaginary frequency of only 6*i* cm^{-1} at the UCCSD(T)-F12b/AVTZ level, and 56*i* cm^{-1} at the RMP2/AVDZ level. This extreme flatness of the imaginary mode explains why previous studies have reported this saddle point as the reactant minimum.

We have also discovered a new stationary point in the reactant region (RCX), with a classical relative energy of −1.0 kcal/mol at the UCCSD(T)-F12b/AVTZ level. Unfortunately, we are unable to confirm that this stationary point is a true minimum, due to Hartree–Fock convergence failures at the displacements of the numerical Hessian calculation that we have been unable to resolve. Performing the ManyHF procedure[59] *de novo* at every displacement generated for the numerical Hessian would likely resolve the issue, but due to technical limitations in Molpro 2015 that is only possible for numerical gradients, not Hessians.

TS1 is the lowest saddle point leading to the ·CH_2OH + H_2O product complex, with a classical relative energy of 1.3 kcal/mol at the UCCSD(T)-F12b/AVTZ level, while TS1b (which corresponds to the higher energy conformer reported by Gao *et al.*[16]) is found at 2.1 kcal/mol.

The lowest saddle point leading to CH_3O· + H_2O (TS2) is arguably the most challenging stationary point of this system, as multireference effects are the most pronounced here. One can find multiple opinions in the literature regarding the necessity of a multireference method for this geometry.

While Gao *et al.*[16] have opted to use the CASPT2 multireference perturbation theory, Roncero *et al.* have argued[17] that the use of single-reference CC methods is justified despite the elevated T_1 and M diagnostics,[91,92] as their MRCI calculations indicate that only two references are important for the ground state energy and they differ in only a single excitation. Nguyen *et al.* have also chosen to use single reference methods in their study of the reaction.[22] In light of this, we have decided to stay consistent and perform the geometry optimization at the UCCSD(T)-F12b/AVTZ level, and found TS2 with a classical relative energy of 4.0 kcal/mol.

We have also attempted to locate the two higher energy conformers of TS2 reported by Gao *et al.*, but we could not fully converge the geometry optimizations at the RMP2/AVDZ level, nor at the RCCSD/AVDZ level, despite considerable effort.

The ·CH_2OH + H_2O and CH_3O· + H_2O product complexes (MC1 and MC2, respectively) were also located, with classical relative energies of −28.7 and −17.7 kcal/mol. It has been proposed[26] that the free CH_3O· radical does not have C_{3v} symmetry due to Jahn–Teller distortion, and our optimized geometry also supports that: two CH bonds have a bond length of 1.095 Å but the third is 1.104 Å long.

The classical reaction energies were determined to be −22.1 kcal/mol for ·CH_2OH + H_2O and −12.6 kcal/mol for CH_3O· + H_2O at the UCCSD(T)-F12b/AVTZ level, while inclusion of Δ_{ZPE} contributions yields the adiabatic reaction energies of −22.7 and −13.7 kcal/mol, as shown in Fig. 1.

B. Product isomerization and H_2CO formation

Given the thermodynamically favorable nature[26,30,31,34,35,93] of the isomerization of the methoxy radical to the hydroxymethyl radical, it is important to calculate any relevant barrier heights. In 2011, Buszek *et al.* proposed[30] that a single water molecule may act as an effective catalyst for the isomerization reaction, which opens the intriguing possibility that the reaction dynamics of reaction Eq. (R1) may also proceed through the initial formation of CH_3O· + H_2O, followed by a water-catalyzed isomerization.

The methoxide and hydroxymethyl radicals are also known[26,31] to be capable of the unimolecular dissociation described by Eqs. (R3) and (R4),

$$CH_3O\cdot = CH_2O + \cdot H, \tag{R3}$$

$$\cdot CH_2OH = CH_2O + \cdot H, \tag{R4}$$

which yields formaldehyde and a hydrogen atom, resulting in the net reaction (R5),

$$CH_3OH + \cdot OH = CH_2O + \cdot H + H_2O, \tag{R5}$$

when combined with (R1) or (R2). It is noteworthy that both dissociation pathways feature a pronounced barrier that rises above

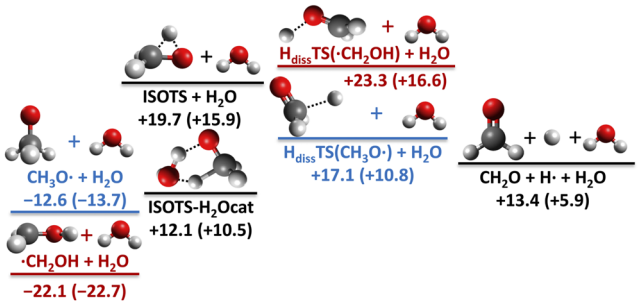

FIG. 2. Relative classical and adiabatic energies of the product isomerization and H_2CO formation pathways of the CH_3OH + ·OH system at the UCCSD(T)-F12b/AVTZ level. Adiabatic energies are given in parentheses, and all energies are in kcal/mol relative to free CH_3OH + ·OH.

the product asymptote of Eq. (R5), which may have an impact on dynamics if it prevents reassociation.

Using the coordinates from Ref. 30 as a starting point, we have found the transition state of uncatalyzed isomerization to have a classical relative energy of 19.7 kcal/mol, while the involvement of water lowered this to 12.1 kcal/mol at the UCCSD(T)-F12b/AVTZ level, as shown in Fig. 2.

The initial geometries for the hydrogen dissociation saddle points were taken from Ref. 31, leading to an optimized classical relative energy of 23.3 kcal/mol for the dissociation TS of $\cdot CH_2OH$ and 17.1 kcal/mol for $CH_3O\cdot$, at the UCCSD(T)-F12b/AVTZ level, while the classical reaction energy of (R5) was found to be 13.4 kcal/mol. It is interesting to note that these results (Fig. 2) indicate that the reverse of (R4) (formation of $\cdot CH_2OH$ from H_2CO + H·) has a higher barrier than the reverse of (R3), even though $\cdot CH_2OH$ is the thermodynamically favored isomer.

Δ_{ZPE} contributions are very pronounced for the hydrogen dissociation geometries, and to a lesser extent for the uncatalyzed isomerization barrier. The adiabatic relative energies are universally lower, resulting in a reaction energy of only 5.9 kcal/mol, and a barrier height of just 10.8 kcal/mol for (R3), suggesting that formaldehyde formation may be an accessible product channel for dynamics.

C. A survey of exotic products

The list of exotic products surveyed is presented in Table I.

Our UCCSD(T)-F12b/AVTZ results are in good agreement with the ATcT reference data, often within its 95% confidence limits. The largest deviations are seen for the CH_4 + ·OOH (0.55 kcal/mol), $\cdot CH_3$ + H_2O_2 (0.30 kcal/mol), and $H_3COO\cdot$ + H_2 (0.34 kcal/mol) product channels, for which additional corrections would be necessary to reach the accuracy of the reference data.

While many of the products considered have very high relative energies, rendering them dynamically inaccessible at reasonable collision energies, there are some noteworthy exceptions,

$$CH_3OH + \cdot OH = CH_2(OH)_2 + \cdot H, \quad \text{(R6)}$$

$$CH_3OH + \cdot OH = CH_2OHO\cdot + H_2. \quad \text{(R7)}$$

The possibility of hydroxymethoxy radical and methanediol formation in CH_3OH + ·OH collisions has only recently been proposed[11] by Inostroza-Pino *et al.*, based on their direct dynamics results on the high-energy ·OH bombardment of methanol ice, but no high-accuracy reaction energies were calculated.

The substitution of a hydrogen atom by the hydroxyl radical to form methanediol [reaction (R6)] is slightly but decisively exothermic (−2.6 kcal/mol), while the formation of the hydroxymethoxy radical alongside dihydrogen [reaction (R7)] is modestly exothermic (−1.7 kcal/mol) once the Δ_{ZPE} contributions are included at the UCCSD(T)-F12b/AVTZ level.

Whether or not these two products are actually formed in bimolecular collisions with any appreciable cross section is of course to be determined by a dynamics study, but their thermodynamic accessibility warrants the evaluation of their energy with the high-accuracy composite scheme detailed in Sec. II.

D. Alternative conformers and saddle points of $\cdot CH_2OH$, $H_2C(OH)_2$ and $H_2COHO\cdot$

As shown in Fig. 3, the hydroxymethyl radical, methanediol, and the hydroxymethoxy radical have additional stationary points beyond their minimal energy conformation.

TABLE I. Classical and adiabatic reaction energies of some exotic product channels of the CH_3OH + ·OH system at the UCCSD(T)-F12b/AVTZ level. All energies are in kcal/mol relative to free CH_3OH + ·OH. The uncertainty estimates of the ATcT reference data correspond to 95% confidence limits.

Products	Classical relative energy	Adiabatic relative energy	ATcT Δ_rH(0 K)
H_3COOH + H (methyl hydroperoxide + H atom)	+64.00	+60.74	+60.68 ± 0.12[94]
C_2–$H_2C(OH)_2$ + H· (methanediol C_2 conformer + H atom)	−1.14	−2.62	−2.52 ± 0.22[95]
C_s–$H_2C(OH)_2$ + H· (methanediol C_s conformer + H atom)	+1.51	−0.30	−0.06 ± 0.22[96]
H_2COO + H_2 + H· (dioxirane + hydrogen + H atom)	+101.23	+90.31	+90.40 ± 0.13[97]
$\cdot CH_3$ + H_2O_2 (methyl radical + hydrogen peroxide)	+43.99	+41.68	+41.39 ± 0.04[98]
$H_3COO\cdot$ + H_2 (methylperoxy radical + hydrogen)	+46.51	+42.22	+41.88 ± 0.09[99]
$\cdot CH_2OOH$ + H_2 (hydroperoxymethyl radical + hydrogen)	+60.00	+54.14	+53.94 ± 0.31[100]
$H_2C(OH)O\cdot$ + H (hydroxymethoxy radical + hydrogen)	+3.10	−1.71	No data
CH_4 + ·OOH (methane + hydroperoxyl radical)	+25.38	+24.77	+24.22 ± 0.05[101]

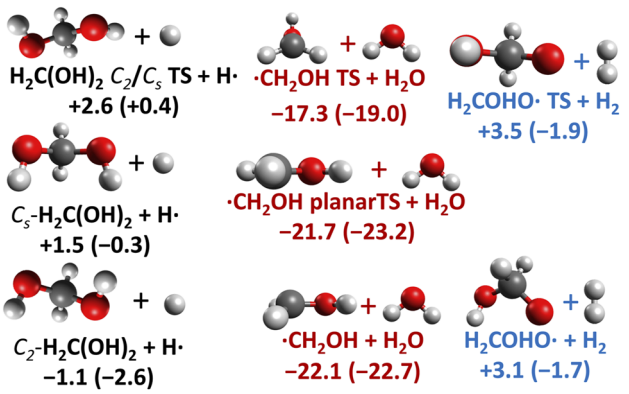

FIG. 3. Relative classical and adiabatic energies of conformational saddle points and minima of the $\cdot CH_2OH$, $H_2C(OH)_2$, and $H_2COHO\cdot$ products at the UCCSD(T)-F12b/AVTZ level. Adiabatic energies are given in parentheses, and all energies are in kcal/mol relative to free $CH_3OH + \cdot OH$.

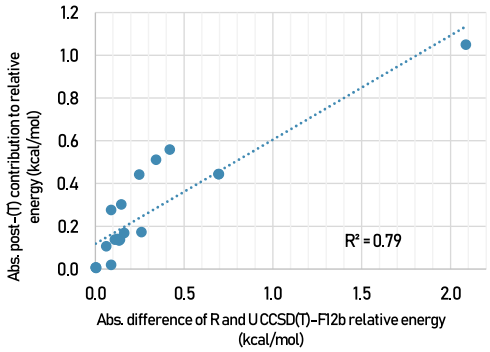

FIG. 4. Absolute difference between ROHF-UCCSD(T)/AVDZ and UHF-UCCSDT(Q)/AVDZ relative energies at ROHF-UCCSD(T)-F12b/AVTZ geometries, in function of the absolute difference between optimized ROHF-RCCSD(T)-F12b/AVTZ and ROHF-UCCSD(T)-F12b/AVTZ relative energies.

In case of the methanediol, the higher energy C_s symmetric conformer is found at a classical relative energy of 1.5 kcal/mol, while the TS connecting the two conformers sits at 2.6 kcal/mol. Upon the inclusion of Δ_{ZPE} contributions these energies change to −0.3 and 0.4 kcal/mol, respectively, corresponding to a 0 K $C_s \rightarrow C_2$ barrier of 0.7 kcal/mol, in excellent agreement with previous calculations.[32]

We have found two conformational saddle points for the hydroxymethyl radical, a non-planar geometry with C_s symmetry at a classical relative energy of −17.3 kcal/mol (4.8 kcal/mol above the minimum geometry of $\cdot CH_2OH$) and a planar C_s symmetric geometry at −21.7 kcal/mol (0.3 kcal/mol above the $\cdot CH_2OH$ minimum).

For the hydroxymethoxy radical, one conformational saddle point was found at 3.5 kcal/mol, 0.4 kcal/mol above its equilibrium geometry.

E. Effects of partially spin-restricted coupled-cluster methods

It is traditionally believed,[37] that the effects of spin-restriction in the CC equations of ROHF-referenced coupled cluster methods are typically negligible for most thermochemical or spectroscopic quantities.

Very recently, a spin-adapted and spin-complete coupled-cluster (SASC-CCSD) method[102] that fully eliminates all remaining spin contamination arising from the cluster and spin operators has been published. The authors have compared the correlation energies obtained with the ROHF-UCCSD and ROHF-SASC-CCSD methods for a few small molecules, found minor to negligible differences, and suggested that the use of SASC-CCSD would only be worthwhile for calculating spin-dependent properties, such as hyperfine coupling tensors.[102]

Our results with the partially spin-restricted coupled cluster methods[37] implemented in Molpro 2015 disagree. The most striking example is TS2, where the classical relative energy of the saddle point is 6.1 kcal/mol if optimized at the RCCSD(T)-F12b/AVTZ level, but 4.0 kcal/mol if optimized at the UCCSD(T)-F12b/AVTZ level. Other examples that stand out to a lesser extent are the two TS1 conformers with an R/U energy difference of 0.7 kcal/mol and the $CH_3OO\cdot + H_2$ product channel with 0.6 kcal/mol. The full table of optimized RCC and UCC relative energies, as well as the Cartesian coordinates of optimized geometries are found in the supplementary material.

While we consider these results surprising and of theoretical interest, investigating the source and significance of this difference is outside of the scope of the present work, especially considering the unavailability of higher-order restricted coupled-cluster methods, such as a hypothetical ROHF-RCCSDT(Q).

With that said, we have performed RCCSD(T)/AVTZ and UCCSD(T)/AVTZ single-point calculations at the UCCSD(T)-F12b/AVTZ geometries of TS1 (and the free reactants) to isolate the R/U relative energy difference from any contribution stemming from geometric differences and F12 terms, and have found the R/U difference in classical relative energies to be 0.64 kcal/mol, almost identical to the difference in optimized classical relative energies. We also observe that there is some correlation (Fig. 4) between the R/U difference of optimized classical relative energies and contributions from post-(T) calculations.

We hope that these results motivate further investigation of the differences between the standard ROHF-UCCSD and the various spin-restricted and spin-adapted CC methods, especially at challenging transition states and in the presence of moderate amounts of static correlation.

IV. BENCHMARK COMPOSITE ENERGY CALCULATIONS

A. Basis set convergence of Hartree–Fock energies and F12 CABS corrections

As shown in Fig. 5, AVTZ on its own does not reach the HF basis set limit, and even with the F12 CABS correction an RMS error of 0.1 kcal/mol is incurred. AVQZ lowers this to 0.037 kcal/mol, but the CABS correction only improves this to 0.029 kcal/mol.

VTZ-F12 is a major improvement over AVTZ even without the CABS correction (0.09 vs 0.17 kcal/mol RMSE), and VTZ-F12 + CABS outperforms even AVQZ + CABS with an RMSE of

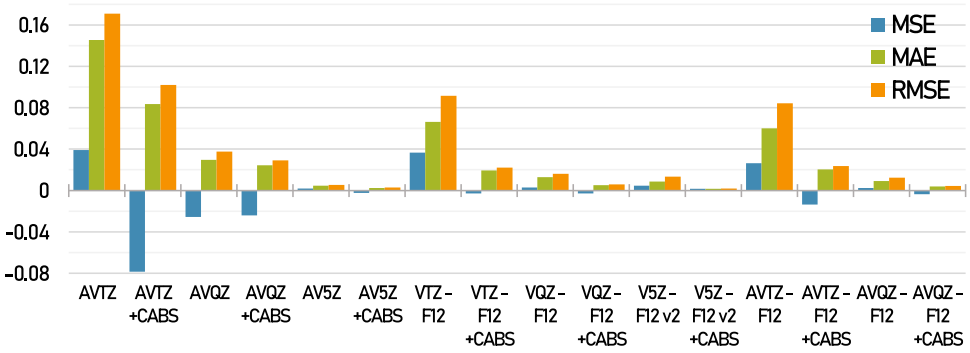

FIG. 5. Mean signed error (MSE), mean absolute error (MAE), and root-mean-square error (RMSE) of the ROHF relative energies of the 19 geometries used for composite calculations, at various basis sets, with and without F12 CABS correction, compared with ROHF/AwCV5Z + CABS reference relative energies. All errors are in kcal/mol.

0.022 kcal/mol, at a much-reduced computational cost (249 vs 470 basis functions). VQZ-F12 + CABS has an RMSE < 0.01 kcal/mol, and is essentially converged to the HF limit at a much-reduced cost compared with AV5Z (431 vs 781 basis functions).

The results with the AV*n*Z-F12 basis sets are very close to the V*n*Z-F12 series, and offer no meaningful improvement to offset their increased cost when it comes to the HF basis set errors of the 19 relative energies tested here.

B. Basis set convergence of valence CCSD-F12b and (T) correlation energies

Basis set errors of the valence CCSD(T) correlation energy are typically the largest sources of error in *ab initio* potential energies, and require impractically huge basis sets to eliminate without basis set extrapolation and/or explicit correlation.

As shown in Fig. 6, using the AVTZ basis set incurs an RMS error of 0.129 kcal/mol in the CCSD-F12b correlation energy contribution to the relative energy of the 19 geometries studied. AVQZ improves this to 0.064 kcal/mol, but it takes the very large AV5Z basis set to bring the RMSE down below 0.02 kcal/mol.

Extrapolating the CCSD-F12b correlation energies from the AV{T,Q}Z pair with an extrapolation exponent of 4.25[84] results in a modest improvement (0.046 kcal/mol RMSE), while the AV{Q,5}Z pair yields relative energy contributions extremely close to the AwCV5Z reference values, both with the theoretically derived[86] extrapolation exponent of 7 and an empirically justified[84] value of 4.9.

The VTZ-F12 basis set performs excellently, nearly matching AVQZ with an RMSE of 0.074 kcal/mol, while containing slightly fewer basis functions than even AVTZ. VQZ-F12 also performs well, more than halving the RMSE of AVQZ with 39 fewer basis functions, but somewhat disappointingly, attempting to further improve this by V{T,Q}Z-F12 CBS extrapolations yields no improvement, regardless of the extrapolation exponent. Results with the V5Z-F12(rev2) basis set are practically indistinguishable from the AwCV5Z reference values, even without extrapolation, while using 142 fewer basis functions.

The AVTZ-F12 basis set is only marginally better than VTZ-F12, but AVQZ-F12 is a noticeable improvement over VQZ-F12 and almost matches AV5Z with an RMSE of 0.019 kcal/mol, while being much smaller (569 vs 781 basis functions). Furthermore, unlike the V{T,Q}Z-F12 pair, the AV{T,Q}Z-F12 pair takes well to extrapolation and reaches the accuracy of an AV{Q,5}Z extrapolation when the extrapolation exponent of 4.6 is used.

Calculating the (T) triples approximation using the AwCV5Z basis set (943 basis functions) proved to be impractical on our hardware, thus we have chosen the L^{-3} extrapolated V{Q,5}Z-F12 (T) contributions as our reference values. The AV{Q,5}Z values were also considered, however, that extrapolation covers more energy (0.54 vs 0.42 kcal/mol RMS), and the AV*n*Z (T) correlation energies appear to be converging from above (Fig. 7) to the V*n*Z-F12 (T) correlation energies.

When it comes to the (T) triples approximation (Fig. 8), using the AVTZ basis set incurs an RMSE of 0.176 kcal/mol, which is reduced to 0.068 kcal/mol by AVQZ and 0.029 kcal/mol by AV5Z.

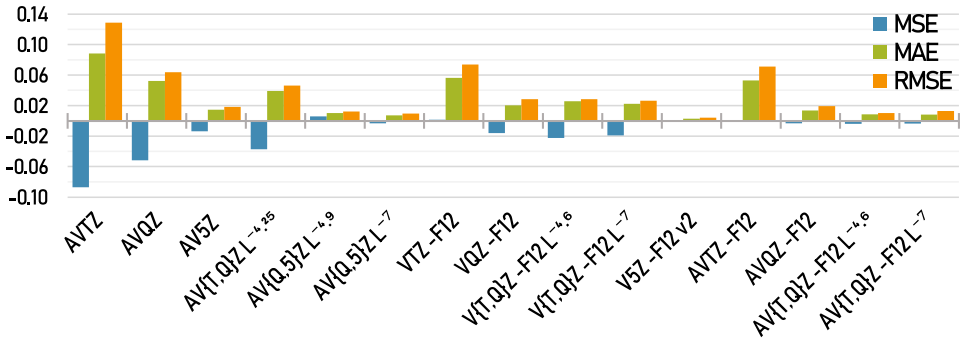

FIG. 6. Mean signed error (MSE), mean absolute error (MAE) and root-mean-square error (RMSE) of the UCCSD-F12b correlation energy contribution to the relative energies of the 19 geometries used for composite calculations, at various basis sets and CBS extrapolations, compared with UCCSD-F12b/AwCV5Z reference relative energies. All errors are in kcal/mol.

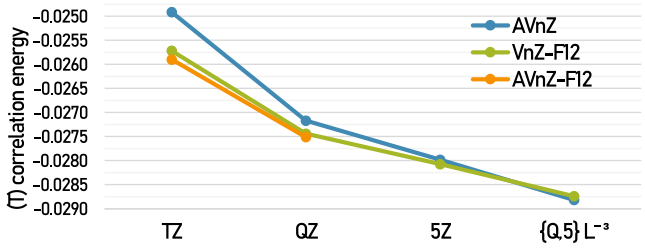

FIG. 7. (T) correlation energies of TS1 using various basis sets and L^{-3} extrapolations from the AV{Q,5}Z and V{Q,5}Z-F12 pairs. (T) correlation energies are taken from UCCSD(T)-F12b calculations at the UCCSD(T)-F12b/AVTZ geometry, and shown in hartrees. This is a representative example of (T) basis convergence at other stationary points.

Performing an AV{T,Q}Z L^{-3} extrapolation yields a major reduction in RMSE, to 0.017 kcal/mol, and a sign change of the MSE, suggesting that the AV{T,Q}Z L^{-3} extrapolation may slightly overshoot the (T)/CBS limit. Surprisingly, there is no advantage to performing a AV{Q,5}Z extrapolation as its results are almost identical to AV{T,Q}Z.

The VTZ-F12 and VQZ-F12 basis sets again outperform AVTZ and AVQZ with 0.13 and 0.049 kcal/mol RMSE, respectively, while using fewer basis functions. A V{T,Q}Z-F12 L^{-3} extrapolation yields a substantial improvement, lowering the RMSE to 0.02 kcal/mol, making it superior to both unextrapolated AV5Z and unextrapolated V5Z-F12(rev2), with a (T)/CBS overshoot similar to AV{Q,5}Z.

Without extrapolation, the increased radial flexibility of AVTZ -F12 and AVQZ-F12 does not lead to worthwhile improvements. This, however, can be changed by applying the simple L^{-3} extrapolation, which is very effective for the AV{T,Q}Z-F12 pair, yielding an RMSE of just 0.013 kcal/mol and outperforming both the AV{Q,5}Z and V{T,Q}Z-F12 extrapolations.

One might wonder if the (often opposite) signs of the basis set errors of the HF, SD, and (T) contributions might lead to fortuitous error cancellation if a convenient "single-shot" CCSD(T)-F12b calculation is used to obtain all contributions without extrapolation.

As can be seen in Fig. 9, for the 19 geometries tested in the present work, the answer seems to be "generally yes," as the total basis set error of a simple CCSD(T)-F12b/AVQZ calculation never exceeds 0.1 kcal/mol, leading to an RMS total basis error of just 0.053 kcal/mol. This, however, can easily be improved further by switching to the VQZ-F12 basis, which reaches an RMSE of 0.035 kcal/mol, by greatly reducing the basis errors of the HF + CABS and CCSD-F12b contributions.

Looking at the rms total basis errors of all basis sets and some extrapolations (Fig. 10), we can make the following observations:

- For single-shot TZ calculations VTZ-F12 performs slightly worse than AVTZ, despite providing HF, CCSD and (T) contributions that are on their own superior in an RMS sense. This can be explained by the upset of error compensation present for AVTZ. AVTZ-F12 is slightly better than AVTZ, however, it has considerably more basis functions (325 vs 253).
- VQZ-F12 is clearly the preferred basis for single-shot QZ calculations, outperforming both AVQZ and AVQZ-F12, with fewer basis functions.
- AV5Z performs marginally better than V5Z-F12 (rev2), again due to error compensation, as V5Z-F12 (rev2) almost completely eliminates the basis error of HF and CCSD contributions, but not of (T).
- Taking the AVTZ/AVQZ pair and separately extrapolating both CCSD and (T) correlations energies with extrapolation exponents of 4.25 and 3, respectively, yields relative energies worse than a single shot AVQZ calculation, despite both extrapolations being beneficial for the extrapolated quantity on their own (Figs. 8 and 9). Doing a similar extrapolation for AV{Q,5}Z is not profitable either.
- The dual extrapolation scheme does, however, perform well with the AV{T,Q}Z-F12 pair, matching the accuracy of AV5Z with fewer basis functions (569 vs 781). Overall, while the improved radial flexibility of the AV*n*Z-F12 series does lead to an improvement, we conclude that the V*n*Z-F12 series is sufficiently diffuse for describing noncovalent interactions between a polar radical and a polar closed shell molecule.
- As the extrapolation of CCSD correlation energy from the V{T,Q}Z-F12 pair offered no benefit (Fig. 7), only the L^{-3} extrapolation of the (T) correlation energy was attempted, which yielded a modest worsening of the total basis error (Fig. 10).

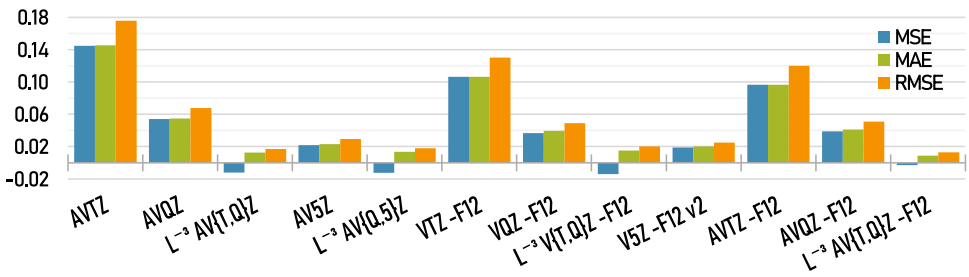

FIG. 8. Mean signed error (MSE), mean absolute error (MAE), and root-mean-square error (RMSE) of the (T) correlation energy contribution to the relative energies of the 19 geometries used for composite calculations, at various basis sets and CBS extrapolations, compared with reference (T) contributions from V{Q,5}Z-F12 L^{-3} extrapolations. All (T) contributions are obtained from UCCSD(T)-F12b calculations, and all errors are in kcal/mol.

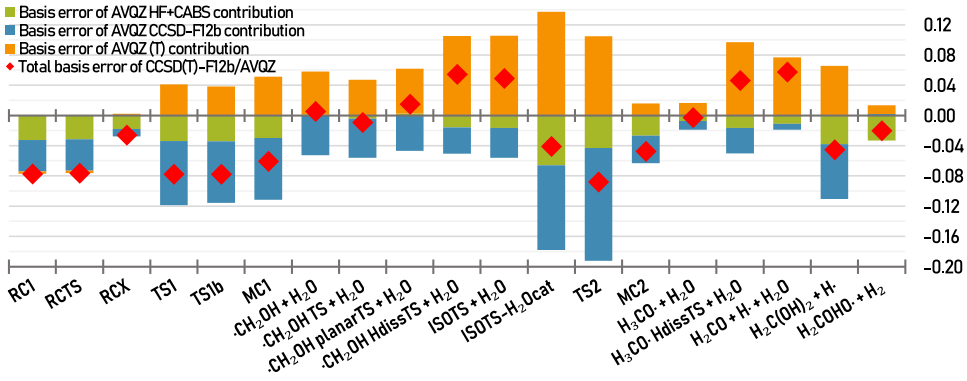

FIG. 9. Basis set errors of the HF + CABS, CCSD-F12b correlation, and (T) correlation energy contributions to the relative energies of the 19 geometries used for composite calculations, as well as the total basis set errors for CCSD(T)-F12b/AVQZ. Reference values for the HF and CCSD-F12b energies are obtained using AwCV5Z, reference (T) contributions are from V{Q,5}Z-F12 L^{-3} extrapolations. All (T) contributions are obtained from UCCSD(T)-F12b calculations, and all errors are in kcal/mol.

C. Pareto efficient basis set choices

The trade-off between computational cost and basis set error is one of the major factors to consider when choosing a basis set. While the choice is usually simple if only a single basis set series is considered (e.g., AVnZ), different basis sets series and extrapolation schemes may, however, differ in how much basis set error is eliminated per basis function.

Such trade-off decisions can be made easier by adopting the concept of Pareto fronts from engineering. A Pareto front can be constructed by finding the set of Pareto optimal choices (in this case, they are the choices where no other option is simultaneously faster and more accurate), which then can be used to aid the choice of basis set.

Since the number of basis functions is the primary factor in the CPU time, memory, and disk requirements of any non-integral-direct CCSD(T) calculation, we have plotted (Fig. 11) the RMS basis set errors in the function of the number of basis functions used, or in case of extrapolations the number of basis functions for the largest basis of the extrapolation.

Such a plot can be interpreted by considering that the ideal basis set would approach zero error with very few basis functions, and thus would be near the bottom left corner of Fig. 11.

D. Post-(T) correlation energies and their reference dependence

Incorporating electron correlation effects beyond the CCSD(T) approximation is an important part of high-accuracy composite schemes. Due to the extreme computational cost of CCSDTQ calculations, the highest feasible level of theory is typically CCSDT(Q) with a modest basis set. Defining the iterative triples contribution $\delta[\mathrm{T}]$ and the noniterative quadruples contribution $\delta[(\mathrm{Q})]$ is straightforward for closed-shell systems, but open-shell systems bring complications.

Assuming that the UCCSD(T)/CBS results are computed using an ROHF reference and the UCCSDT(Q) calculations use the AVDZ basis set one can define $\delta[\mathrm{T(Q)}]$ [the total post-(T) correction] four different ways,

$$\mathrm{I.}\quad \delta[\mathrm{T(Q)}] = E\big(\mathrm{ROHF\text{-}UCCSDT(Q)}_{/\mathrm{A}}/\mathrm{AVDZ}\big) - E(\mathrm{ROHF\text{-}UCCSD(T)/AVDZ}),$$

$$\mathrm{II.}\quad \delta[\mathrm{T(Q)}] = E\big(\mathrm{ROHF\text{-}UCCSDT(Q)}_{/\mathrm{B}}/\mathrm{AVDZ}\big) - E(\mathrm{ROHF\text{-}UCCSD(T)/AVDZ}),$$

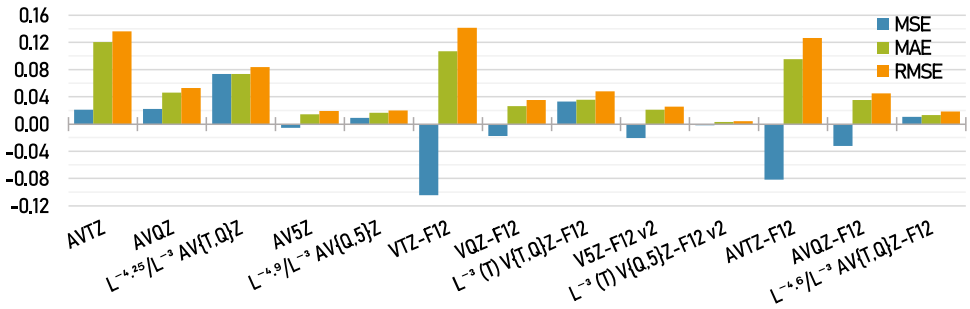

FIG. 10. Mean signed error (MSE), mean absolute error (MAE), and root-mean-square error (RMSE) of the relative energies of the 19 geometries used for composite calculations, at various basis sets and CBS extrapolations, compared with our best estimates for the CCSD(T)/CBS relative energies. L^{-a}/L^{-b} denote separate extrapolations of the CCSD-F12b and (T) correlation energies, L^{-b} (T) indicates only the (T) correlation energy is extrapolated. All errors are in kcal/mol.

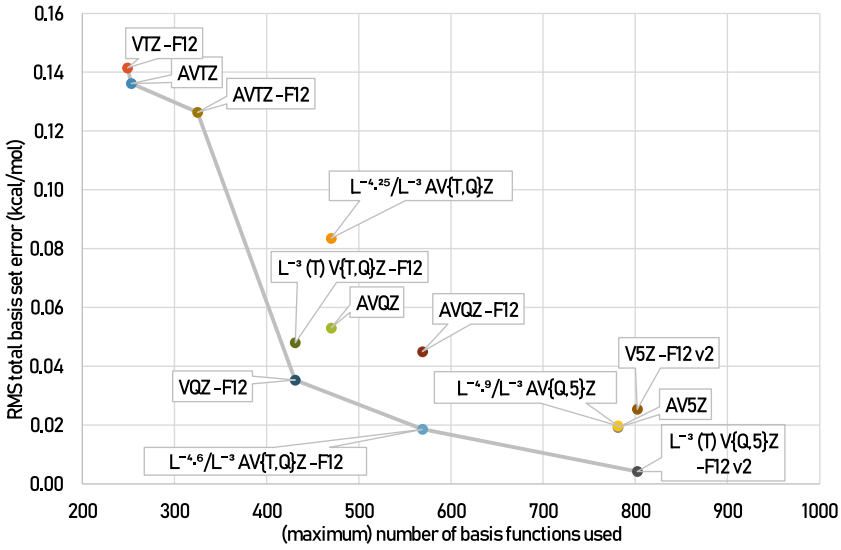

FIG. 11. RMS total basis set error of the relative energies of the 19 geometries used for composite calculations, compared with our best estimates for the CCSD(T)/CBS relative energies, in function of basis size. L^{-a}/L^{-b} denote separate extrapolations of the CCSD-F12b and (T) correlation energies, L^{-b} (T) indicates only the (T) correlation energy is extrapolated. All errors are in kcal/mol, for extrapolations, the size of the larger basis is used.

III. $\delta[\mathrm{T(Q)}] = E(\mathrm{UHF\text{-}UCCSDT(Q)/AVDZ}) - E(\mathrm{ROHF\text{-}UCCSD(T)/AVDZ})$,

IV. $\delta[\mathrm{T(Q)}] = E(\mathrm{UHF\text{-}UCCSDT(Q)/AVDZ}) - E(\mathrm{UHF\text{-}UCCSD(T)/AVDZ})$.

The most consistent option is of course to use the same ROHF wavefunction for all CC calculations regardless of excitation level (options I and II), in which case the ambiguity comes from the non-uniqueness in the definition of the (Q) equations.[55] For technical reasons (such as interface limitations between the MRCC package and other programs), the use of options III and IV may be required, which may lead to different post-(T) corrections. As there is some evidence[73] that the $(Q)_{/B}$ variant is a more robust approximation, option I is given no further consideration in this work.

TABLE II. Post-(T) contributions to the relative energies of the 19 geometries used for composite calculations and values of the UHF spin-squared operator. The post-(T) contributions are calculated from ROHF- and UHF-referenced UCCSDT(Q)/AVDZ results at UCCSD(T)-F12b/AVTZ geometries and are in kcal/mol.

Geometry	$\delta[\mathbf{T(Q)}]$ option III [R(T) → UT(Q)]	$\delta[\mathbf{T(Q)}]$ option IV [U(T) → UT(Q)]	UHF $\hat{S}^2$	$\delta[\mathbf{T(Q)}]$ option II [R(T) → RT(Q)$_{/B}$]
RC1	−0.01	−0.01	0.756	0.02
RCTS	−0.01	−0.01	0.756	0.02
RCX	−0.01	−0.01	0.757	0.02
TS1	−0.45	−0.47	0.771	−0.38
TS1b	−0.44	−0.47	0.770	−0.37
MC1	−0.13	−0.16	0.762	−0.08
·CH_2OH + H_2O	−0.14	−0.16	0.762	−0.11
·CH_2OH TS + H_2O	−0.11	−0.12	0.761	−0.09
·CH_2OH planarTS + H_2O	−0.14	−0.16	0.764	−0.11
·CH_2OH HdissTS + H_2O	−0.56	−0.75	0.957	−0.49
ISOTS + H_2O	−0.30	−0.38	0.796	−0.29
ISOTS-H_2Ocat	−0.44	−0.50	0.769	−0.35
TS2	−1.05	−0.78	0.785	−0.89
MC2	−0.17	−0.18	0.760	−0.13
H_3CO· + H_2O	−0.14	−0.15	0.760	−0.13
H_3CO· HdissTS + H_2O	−0.51	−0.69	0.923	−0.44
H_2CO + H· + H_2O	−0.28	−0.29	0.75	−0.31
$H_2C(OH)_2$ + H·	0.02	0.00	0.75	−0.01
H_2COHO· + H_2	−0.17	−0.19	0.761	−0.11

Looking at the total post-(T) contributions to the relative energies of the 19 geometries used for composite calculations, calculated with options II, III, and IV (Table II) it is apparent that while in many cases the differences are small (often no more than 0.05 kcal/mol), there are some noticeable deviations.

The largest differences between the UHF-only (option IV) results, and the mixed reference (option III) results are seen at the two hydrogen dissociation saddle points (~0.17 kcal/mol) and at TS2 (0.29 kcal/mol), while the difference is no more than 0.06 kcal/mol for all other geometries.

Between option IV and the ROHF-only option II, the largest difference (~0.26 kcal/mol) is seen for the hydrogen dissociation geometries, TS2 differs by 0.11 kcal/mol, ISOTS-H_2Ocat by 0.15 kcal/mol, TS3 by 0.1 kcal/mol, while the difference is < 0.1 kcal/mol for the rest of the geometries.

The cause of these differences is immediately apparent for the hydrogen dissociation saddle points: the UHF reference is spin-contaminated (Table II). For other geometries, the spin contamination is modest ($\hat{S}^2$ never exceeds 0.8) and other explanations should be sought. TS2 has the most multireference character among the geometries and this is likely responsible to its sensitivity to the ROHF/UHF choice.

These differences underline the importance of clearly specifying the type of reference wavefunction used for open-shell systems. For the sake of consistency with our ROHF-based CCSD(T)-F12 calculations, we have used the ROHF-UCCSDT(Q)$_{/B}$ results in our composite energy scheme.

The importance and makeup of post-(T) corrections vary wildly among the 19 geometries (Fig. 12), but δ[T(Q)] almost universally lowers the relative energies. In the reactant complex region both δ[T] and δ[(Q)] are close to zero, the ·CH_2OH + H_2O product side has a modest (~−0.1 kcal/mol) δ[(Q)] contribution, while the CH_3O· + H_2O minimum and products are stabilized by 0.13 kcal/mol, coming primarily from δ[T].

TS1, TS1b, the two isomerization TSs, the two H· dissociation TSs and the H_2CO + H· + H_2O products all have more pronounced δ[T(Q)] corrections in the −0.3 to −0.5 kcal/mol range, with the δ[(Q)] contribution typically having more impact. At this point, it is perhaps worth remembering, that the peak basis set error of a straightforward FC-UCCSD(T)-F12b/VQZ-F12 calculation is under 0.1 kcal/mol for the 19 geometries, making the post-(T) contributions far more impactful than any further improvement to the valence correlation energy.

As expected, δ[T(Q)] is the most important at TS2, reaching −0.89 kcal/mol, with roughly $^2/_3$ of that coming from δ[T].

E. Core correlation, scalar relativistic, and spin–orbit coupling corrections

While the frozen-core approximation is typically not a major source of error for systems composed of first-row elements, core correlation cannot be entirely neglected for high-accuracy thermochemistry. The total contribution of core correlation to the relative energies (Fig. 13) ranges from negligible to −0.23 kcal/mol and typically lowers the relative energies, with an RMS contribution of 0.11 kcal/mol over the 19 geometries. The primary component of the Δ_{core} contribution can be either the CCSD-F12b correlation energy, the (T) contribution, or both, depending on the geometry.

As expected for first row elements, scalar relativistic effects are also modest in magnitude, no more than 0.14 kcal/mol, with the overwhelming majority of the relativistic contribution already captured at the CCSD level. The sign of Δ_{rel} is typically the opposite of Δ_{core}, thus they largely cancel each other out and the sum of Δ_{core} + Δ_{rel} never exceeds 0.1 kcal/mol (Fig. 13).

For most geometries (Fig. 14) the contribution of Δ_{SO} is near 0.2 kcal/mol, corresponding to the complete cessation of the spin–orbit coupling found in a free ·OH radical, with the exception of the three reactant complex geometries. RC1 and RCTS lose roughly half of the spin–orbit interaction energy, while the much more loosely associated RCX retains almost all of the spin–orbit coupling of the free ·OH.

While the calculated spin–orbit splitting of the hydroxyl radical (138.3 cm^{-1}) is very close to the correct value[103] of 139.2 cm^{-1}, calculating the precise energy difference between the nonrelativistic ground state and the spin–orbit ground state is a thorny issue for ·OH, as the spin–orbit coupling further extends to couple with the molecular rotation of a free ·OH, resulting in a non-zero rotational zero-point energy,[103] raising the lowest allowed energy level of OH by 31.4 cm^{-1} (0.0898 kcal/mol).

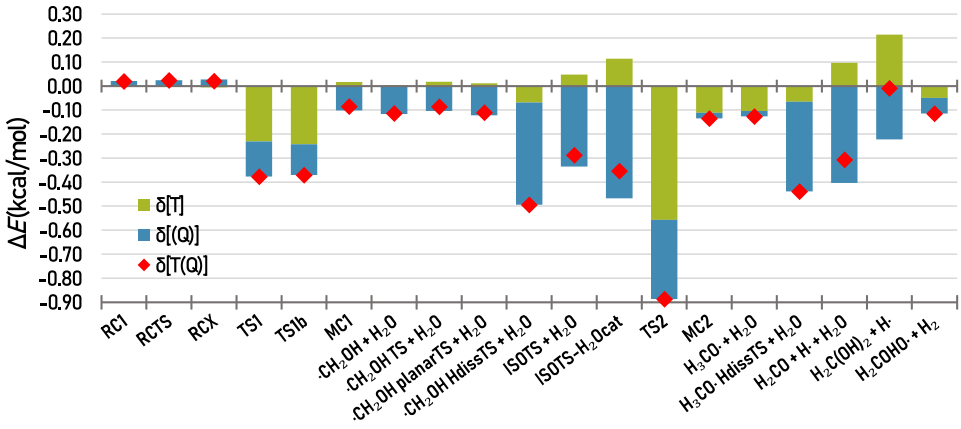

FIG. 12. Post-(T) corrections [Eqs. (3) and (4)] to the relative energies.

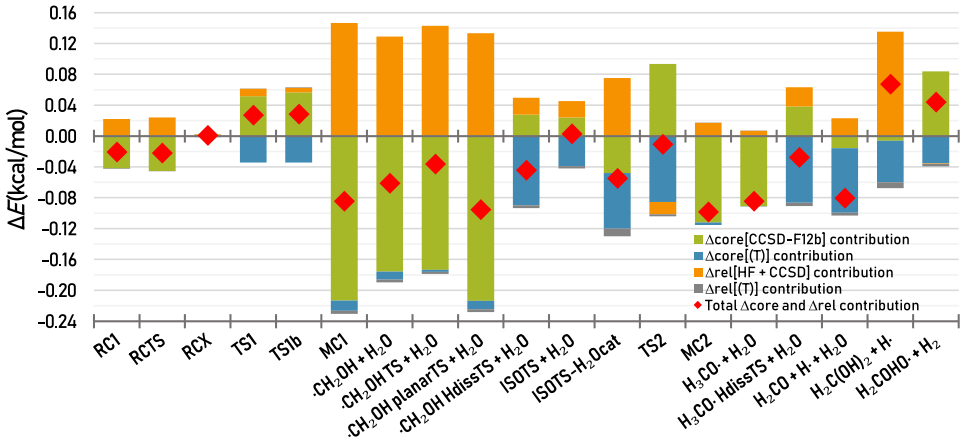

FIG. 13. Core correlation [Eq. (5)] and scalar relativistic [Eq. (6)] corrections to the relative energies.

As this contribution is only known for free ·OH (and would likely be unfeasible to attempt to calculate *ab initio*), the only straightforward way to incorporate it into our results is to assume, that none of the 19 geometries has any rotational zero-point energy, not even at the reactant complexes, where much of the SO coupling is still present. Under this assumption, the OH rotational ZPE (rZPE) would be just an additional flat −0.0898 kcal/mol contribution to the relative energies.

F. Vibrational zero-point energy contributions

The inclusion of vibrational zero-point energy (ZPE) contributions can substantially alter the relative energy landscape, especially when bonds between hydrogen atoms and heavy atoms are made or broken.

The inclusion of the Δ_{ZPE} contributions (Fig. 15) has a wildly different effect, depending on the geometry in question. The reactant and product complexes are destabilized by a relatively modest amount (0.8–1.8 kcal/mol), while most other geometries are stabilized by a similar amount.

The most notable exceptions to this are the three geometries of the formaldehyde formation pathway, where the two hydrogen dissociation saddle points are stabilized by 6.7 and 6.3 kcal/mol, and the $H_2CO + H\cdot + H_2O$ products by 7.5 kcal/mol. Δ_{ZPE} also stabilizes the product isomerization saddle point and the $H_2COHO\cdot + H_2O$ product channel by 3.9 and 4.8 kcal/mol, respectively.

G. Final classical and adiabatic benchmark results, comparison with literature data

Summing up all of the contributions and corrections discussed *vide supra*, we arrive at our best estimates for the classical and adiabatic relative energies of the 19 geometries (Table III).

In general, using the high-accuracy composite scheme described in Sec. II brings no qualitative changes to the FC-UCCSD(T)-F12b/AVTZ results discussed in Sec. III, but there are notable quantitative changes at some of the energies, and our results can be compared with values gathered from the literature (Table IV).

For the reactant complex (RC1), our classical relative energy value of −6.31 kcal/mol is in excellent agreement with previous results from Gao *et al.*,[16] Roncero *et al.*[17] and Nguyen *et al.*[22] (−6.48, −6.46, and −6.15 kcal/mol).

Including the vibrational ZPE contribution (Δ_{ZPE}) and the rotational ZPE correction discussed in Sec. IV E yields our adiabatic relative energy of −4.59 kcal/mol, which is well within the uncertainty estimate of −4.37 ± 0.48 kcal/mol from Ref. 22, and is also compatible with −4.75 ± 0.5 kcal/mol reported by Ocaña *et al.*[23]

While there is no directly comparable literature data for RCTS and RCX, we believe our results at those geometries to be similarly accurate. Overall, at the three reactant complex geometries, given the small values of post-(T), core-correlation, and scalar relativistic corrections (Table III), the primary sources of remaining error in our adiabatic relative energies are expected be the treatment of the

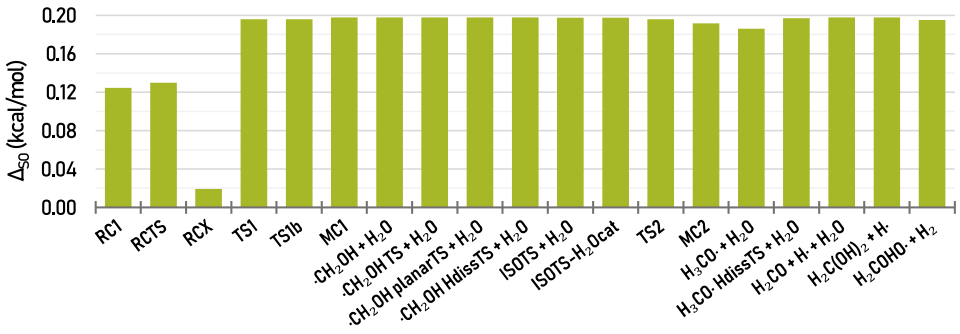

FIG. 14. Spin–orbit coupling [Eq. (7)] correction to the relative energies.

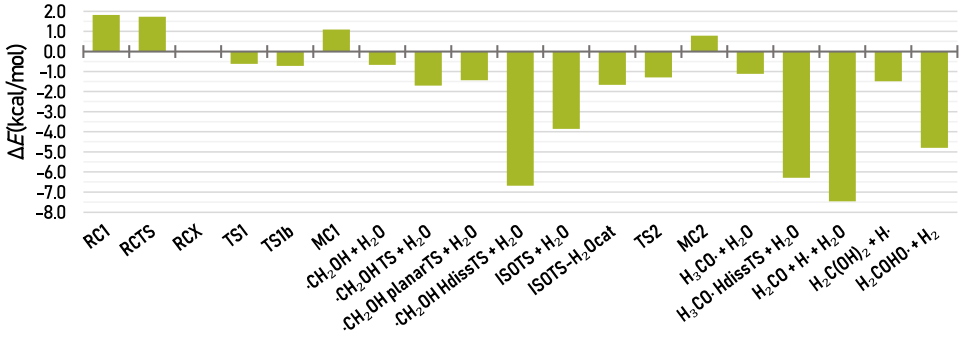

FIG. 15. Harmonic vibrational zero-point energy contributions to the adiabatic relative energies.

spin–orbit coupling (including the problem of rotational ZPE) and the harmonic approximation in the vibrational ZPE calculation.

For TS1, our classical energy is 1.27 kcal/mol, in excellent agreement with the 1.20 kcal/mol of Ref. 22 and the 1.46 kcal/mol of Ref. 16. These results disagree with the results of Refs. 17 and 15, which predict 2.14 and 2.1 kcal/mol, respectively. In the case of Ref. 17, the difference may be explained by their choice to use the partially spin-restricted RCCSD(T)-F12a method, as our RCCSD(T)-F12b energy (Table S1) for TS1 is 0.7 kcal/mol higher than our UCCSD(T)-F12b energy.

Our adiabatic energy for TS1 (0.55 kcal/mol) is again within the uncertainty estimates of the results from both Ref. 22 (0.10 ± 0.48 kcal/mol) and Ref. 23 (0.98 ± 0.5 kcal/mol).

For the higher energy TS1b conformer, our classical and adiabatic energies are 2.09 and 1.28 kcal/mol, respectively. This classical energy is in excellent agreement with the 2.29 kcal/mol reported in Ref. 16. For TS1 and TS1b the primary remaining sources of error are expected to be the neglect of ultra-high-order, post-(Q) coupled-cluster contributions beyond CCSDT(Q), the basis set error of the $\delta[T(Q)]$ correction and the harmonic approximation in the vibrational ZPE calculation.

Our classical and adiabatic energies for the hydroxymethyl product complex (MC1) are −28.65 and −27.66 kcal/mol, which are expected to be more accurate than the −27.7 and −26.7 kcal/mol obtained by Xu and Lin. We predict a 0 K reaction enthalpy of −22.94 kcal/mol for the free $\cdot CH_2OH + H_2O$ products, in excellent

TABLE III. Benchmark composite classical [Eq. (1)] and adiabatic [Eq. (8)] relative energies and their makeup. All energies are in kcal/mol and relative to free $CH_3OH + \cdot OH$. For RCX, no adiabatic energy is available due to convergence issues in the numerical hessian calculation.

Geometry	E(UCCSD-F12b/AwCV5Z)	δ[(T)/CBS]	δ(T)	δ[(Q)]	Δ_{core}	Δ_{rel}	Δ_{SO}	Classical relative energy	Difference from UCCSD(T)-F12b/AVTZ	Δ_{ZPE}	Adiabatic relative energy	Adiabatic relative energy with rZPE
RC1	−6.13	−0.30	0.00	0.02	−0.04	0.02	0.12	−6.31	0.32	1.8	−4.50	−4.59
RCTS	−6.14	−0.29	0.00	0.02	−0.04	0.02	0.13	−6.29	0.32	1.7	−4.56	−4.65
RCX	−0.78	−0.14	−0.01	0.03	0.00	0.00	0.02	−0.88	0.13	NoCo	N/A	N/A
TS1	3.84	−2.42	−0.23	−0.15	0.02	0.01	0.20	1.27	−0.02	−0.6	0.64	0.55
TS1b	4.59	−2.35	−0.24	−0.13	0.02	0.01	0.20	2.09	−0.01	−0.7	1.37	1.28
MC1	−26.86	−1.83	0.02	−0.10	−0.23	0.14	0.20	−28.65	0.08	1.1	−27.57	−27.66
$\cdot CH_2OH + H_2O$	−20.77	−1.42	0.00	−0.12	−0.19	0.13	0.20	−22.17	−0.11	−0.7	−22.85	−22.94
$\cdot CH_2OH$ TS + H_2O	−16.30	−1.08	0.02	−0.10	−0.18	0.14	0.20	−17.31	−0.02	−1.7	−19.01	−19.10
$\cdot CH_2OH$ planarTS + H_2O	−20.46	−1.45	0.01	−0.12	−0.22	0.13	0.20	−21.92	−0.18	−1.4	−23.35	−23.44
$\cdot CH_2OH$ HdissTS + H_2O	27.09	−3.93	−0.07	−0.43	−0.06	0.02	0.20	22.82	−0.50	−6.7	16.13	16.04
ISOTS + H_2O	22.93	−3.31	0.05	−0.34	−0.01	0.02	0.20	19.53	−0.21	−3.9	15.67	15.58
ISOTS-H_2Ocat	18.32	−6.05	0.11	−0.47	−0.12	0.07	0.20	12.05	−0.09	−1.7	10.39	10.30
TS2	8.53	−4.23	−0.56	−0.33	0.01	−0.02	0.20	3.60	−0.41	−1.3	2.30	2.21
MC2	−16.72	−0.91	−0.11	−0.02	−0.12	0.02	0.19	−17.67	0.06	0.8	−16.88	−16.97
$H_3CO\cdot + H_2O$	−12.19	−0.44	−0.10	−0.02	−0.09	0.01	0.19	−12.65	−0.05	−1.1	−13.77	−13.86
$H_3CO\cdot$ HdissTS + H_2O	20.57	−3.61	−0.06	−0.37	−0.05	0.02	0.20	16.70	−0.39	−6.3	10.40	10.31
$H_2CO + H\cdot + H_2O$	16.08	−2.84	0.10	−0.40	−0.10	0.02	0.20	13.05	−0.31	−7.5	5.58	5.49
$H_2C(OH)_2 + H\cdot$	1.49	−2.60	0.21	−0.22	−0.06	0.13	0.20	−0.86	0.28	−1.5	−2.34	−2.43
$H_2COHO\cdot + H_2$	4.53	−1.41	−0.05	−0.07	0.05	0.00	0.20	3.24	0.15	−4.8	−1.56	−1.65

TABLE IV. Comparison of relative classical (and adiabatic) energies of stationary points leading to $CH_3O\cdot$ and $\cdot CH_2OH$ formation reported in the literature. All values are in kcal/mol relative to free reactants, adiabatic (ZPE-inclusive) energies are in parentheses (**NC:** not computed **NP:** computed, but not published **NF:** stationary point not found).

Geometry	Xu and Lin[15]	Gao *et al.*[16]	Roncero *et al.*[17]	Nguyen *et al.*[22]	Ocaña *et al.*[23]	This work
Reactant complex	−6.8 (−4.9)[a]	−6.48 (−4.92)[b,c,d]	−6.46 (NP)[e]	−6.15 (−4.37 ± 0.48)[f]	NP (−4.75 ± 0.5)[g]	−6.31 (−4.59)
Lowest TS leading to $\cdot CH_2OH + H_2O$	2.1 (1.0)[a]	1.46 (0.52)[b,c]	2.14 (NP)[e]	1.20 (0.10 ± 0.48)[f]	NP (0.98 ± 0.5)[h]	1.27 (0.55)
Second TS leading to $\cdot CH_2OH + H_2O$	NC	2.29 (NP)[b,i]	NC	NC	NC	2.09 (1.28)
Lowest TS leading to $CH_3O\cdot + H_2O$	4.8 (3.6)[a]	3.06 (1.23)[j,c]	6.23 (NP)[e]	3.90 (1.92 ± 0.48)[f]	NP (3.13 ± 0.5)[h]	3.60 (2.21)
Second TS leading to $CH_3O\cdot + H_2O$	NC	10.25 (NP)[j,i]	NC	NC	NC	NF
Third TS leading to $CH_3O\cdot + H_2O$	NC	11.52 (NP)[j,i]	NC	NC	NC	NF
$\cdot CH_2OH + H_2O$ product complex	−27.7 (−26.7)[a]	NP[k]	NC	NC	NC	−28.65 (−27.66)
$CH_3O\cdot + H_2O$ product complex	−17.8 (−16.8)[a]	NP[k]	NC	NC	NC	−17.67 (−16.97)

[a]Relative energies reported by Xu and Lin are assumed to be ZPE-inclusive, classical energies shown here are calculated by subtracting ZPE data found in the supplementary of Ref. 15. Computed at the CCSD(T)/6-311+G(*3df,2p*)//MP2/6-311+G(*3df,2p*) level. The type of reference wavefunction and the precise MP2/CC flavor was not specified by the authors.

[b]Classical energies are computed at the ROHF-UCCSD(T)-F12a/jun-cc-pVTZ//UKS(M08-HX)/6-311+G(*2df,2p*) level.

[c]Adiabatic energies are calculated by obtaining the SRP-scaled ZPE contribution as the difference of the classical and 0 K relative energies from Table 6 of Ref. 16, and adding this to the classical energy.

[d]For the reactant complex, two slightly different ZPE contributions can be calculated based on data from Table 6 of Ref. 16: 1.62 and 1.51 kcal/mol. As neither value is clearly more reliable, we are using their average here.

[e]Computed at the ROHF-RCCSD(T)-F12a/cc-pVDZ-F12 level.

[f]Classical energies are calculated by subtracting the δE(ZPE) and OH rotational ZPE (0.09 kcal/mol) contributions from the total mHEAT values of Ref. 22. Uncertainty figure is the estimated uncertainty of mHEAT from Ref. 22.

[g]Computed at the CCSD(T)/CBS(DTQ)//M06-2X/aug-cc-pVQZ level. Ocaña *et al.* estimate in Ref. 23 that their methodology has an uncertainty of 0.5 kcal/mol.

[h]Computed at the CCSD(T)/CBS(DTQ)//IRCMax(CCSD(T)/aug-cc-pVTZ//M06-2X/aug-cc-pVQZ) level. Ocaña *et al.* estimate in Ref. 23 that their methodology has an uncertainty of 0.5 kcal/mol.

[i]No ZPE or frequency data were published for the higher-energy saddle points.

[j]Classical energies are computed at the CASPT2(11,11)/6-311+G(*2df,2p*)//UKS(M08-HX)/6-311+G(*2df,2p*) level.

[k]Gao *et al.* performed the geometry optimization at the UKS(M08-HX)/6-311+G(*2df,2p*) level, followed by a CCSD/jun-cc-pVTZ energy computation, but no energies or complete geometries have been published.

agreement with −23.09 ± 0.06 kcal/mol from[104] the ATcT 1.122r thermochemical network.

We calculate the classical energy of the planar saddle point of free $\cdot CH_2OH$ (associated with the inversion[26] of $\cdot CH_2OH$) to be 0.25 kcal/mol above the equilibrium structure, while the classical barrier of internal rotation is 4.87 kcal/mol. These classical barriers are expected to be more accurate than previous results from the literature.

For MC1, $\cdot CH_2OH + H_2O$ and the two conformational saddle points of $\cdot CH_2OH$ all remaining errors in the classical energies are expected to be small, making the harmonic oscillator approximation of the ZPE the weakest link for adiabatic energies, especially for planar $\cdot CH_2OH$, where the adiabatic energy of the inversion saddle point lays below the adiabatic energy of the $\cdot CH_2OH$ minimum.

Our adiabatic barrier height for the uncatalyzed $\cdot CH_2OH \rightarrow CH_3O\cdot$ isomerization is 38.52 kcal/mol relative to free $\cdot CH_2OH$, which is in excellent agreement with the RCCSD(T)/AV{T,Q}Z//RCCSD(T)/AVTZ result (38.90 kcal/mol) from Ref. 31 and also agrees well with literature results of 37.9 and 38.8 kcal/mol.[30,35]

For water catalyzed isomerization, our adiabatic barrier relative to $\cdot CH_2OH$ is 33.24 kcal/mol, in excellent agreement with 33.4 kcal/mol from Ref. 30 but disagreeing with 30.8 kcal/mol from Ref. 35.

The (T) contributions to the isomerization barriers are rather large (Table III), in fact, ISOTS-H_2Ocat has the largest (T) contribution out of all 19 geometries, and the (T) basis set error of VQZ-F12 is the largest (0.11 kcal/mol vs our CBS result) at ISOTS-H_2Ocat, suggesting a slower basis set convergence at this particular geometry. The magnitude of post-(T) corrections is also elevated. Based on this, the primary sources of remaining error are the neglect of post-(Q) corrections, the basis set error of the δ[(T)/CBS] and δ[T(Q)] contributions and the harmonic approximation in the vibrational ZPE calculation. Still, barring the upset of a fortuitous error cancellation between errors in the classical energy and Δ_{ZPE}, we consider our results more reliable.

Literature results disagree with each other strongly regarding the energy of TS2, the most important saddle point leading to $CH_3O\cdot$ formation. As discussed in Sec. III A, this geometry is known to

have moderate multireference character, making the exact choice of electronic structure method highly impactful. Our classical and adiabatic energies of 3.60 and 2.21 kcal/mol agree well with the results from Ref. 22 (3.90 and 1.92 ± 0.48 kcal/mol), and while that is reassuring, the wide spread of literature results should prompt one to ponder the source of these discrepancies.

The easiest result to explain is the 6.2 kcal/mol classical energy from Ref. 17, as they have used the partially restricted CC method, which (as discussed in Sec. III E) yields a relative energy ~2.1 kcal/mol higher. Subtracting this would bring their result roughly in line with other results. Gao *et al.* obtained their classical energy of 3.06 kcal/mol via CASPT2(11,11)/6-311+G(2df,2p), which should be able to adequately treat the static correlation present at this geometry, but may miss some of the dynamic correlation. They have published the convergence of the TS2 classical energy with respect to the size of the active space (Table S4 in Ref. 16), and somewhat reassuringly this was found to be between 2.56 and 4.16 kcal/mol, depending on the active space. In light of these results, the energies reported by Xu and Lin appear to be too high.

Given the very large, −0.89 kcal/mol $\delta[T(Q)]$ correction for TS2 and its moderate multireference character, we expect that the neglect of post-(Q) contributions and the basis set error of the $\delta[T(Q)]$ corrections are the primary remaining sources of error in our energies, with smaller possible contributions from the neglect of diagonal Born–Oppenheimer correction (DBOC) and anharmonicity.

The $CH_3O\cdot + H_2O$ product complex (MC2) is far better behaved than the unruly transition state leading to it. Our classical and adiabatic energies of −17.67 and −16.97 kcal/mol are in excellent agreement with −17.8 and −16.8 kcal/mol from Ref. 15. We predict a 0 K reaction enthalpy of −13.86 kcal/mol for the free $CH_3O\cdot + H_2O$ products, in excellent agreement with −13.71 ± 0.06 kcal/mol from[105] the ATcT 1.122r thermochemical network. The primary source of remaining error is expected to be anharmonicity for both MC2 and the free products.

Our adiabatic barrier height for hydrogen dissociation from $\cdot CH_2OH$ is 38.97 kcal/mol relative to free $\cdot CH_2OH$, dissociation from $CH_3O\cdot$ involves a 24.17 kcal/mol barrier relative to free $CH_3O\cdot$. This is in good agreement with 39.95 and 24.66 kcal/mol from Ref. 31, and the primary error sources are expected to be anharmonicity and the basis set error of the $\delta[(Q)]$ correction. Relative to free $CH_3OH + \cdot OH$, the adiabatic barriers are only 16.04 and 10.31 kcal/mol, which suggests that $CH_2O + \cdot H + H_2O$ may be a dynamically accessible product channel at reasonable collision energies if reactions (R1) and (R2) produce (ro)vibrationally hot $\cdot CH_2OH$ and especially $CH_3O\cdot$.

The formaldehyde product channel has a classical energy of 13.05 kcal/mol, which is lowered to only 5.49 kcal/mol by the large Δ_{ZPE} contribution stemming from CH/OH bond count change. This agrees well with the ATcT 1.122r value[106] of 5.86 ± 0.04 kcal/mol, and the primary source of error is likely to be the harmonic approximation in the Δ_{ZPE} contribution. Indeed, adding the VSCF/VCI anharmonic correction of +0.44 kcal/mol from Ref. 31 to our adiabatic energy would land us at 5.93 kcal/mol, extremely close to the ATcT value.

Our adiabatic energy for the $CH_2(OH)_2 + \cdot H$ product channel is −2.43 kcal/mol, well within the uncertainty of the ATcT 1.122r value[95] of −2.52 ± 0.22 kcal/mol. We can also calculate the 0 K reaction enthalpy of water addition to formaldehyde [$CH_2O + H_2O \rightarrow CH_2(OH)_2$] to be −7.93 kcal/mol. For the $CH_2OHO\cdot + H_2$ product channel, our classical reaction energy is 3.24 kcal/mol, which is lowered to −1.65 kcal/mol by the ZPE contributions. There are no data for the hydroxymethoxy radical in the ATcT database. We expect our results for both of these product channels to be quite accurate, with anharmonicity being the primary source of the remaining error.

V. SUMMARY AND CONCLUSIONS

We have performed a comprehensive, high-accuracy survey of the potential energy landscape of H_5O_2C systems, starting from the perspective of the $CH_3OH + \cdot OH$ reaction, but branching out to also include the conformational saddle points of possible products as well as a number of hypothetical product channels. Our geometry optimizations support that the RC1 reactant complex is non-symmetric and we have found a new stationary point (RCX) in the reactant region. We could not find the two higher energy conformers of TS2 previously reported[16] in the literature. In total, we optimized 28 + 1 geometries (+1 being $CH_3OH + \cdot OH$) at the UCCSD(T)-F12b/AVTZ level, allowing us to evaluate the thermodynamic feasibility of nine unconventional product channels of the $CH_3OH + \cdot OH$ reaction.

Using these preliminary results and the optimized geometries, we have chosen 19 + 1 geometries for detailed study in a combined effort to both obtain very high accuracy thermochemical data and refine the methodology of composite thermochemical schemes for open-shell systems.

We have found that relative energies calculated with the partially spin-restricted ROHF-RCCSD(T)-F12b method can deviate from ROHF-UCCSD(T)-F12b results by as much as 2.1 kcal/mol. We have also investigated the influence of spin-restriction in the reference wavefunctions of UCCSDT(Q) calculations used in high-accuracy composite thermochemical protocols, and we have found that post-(T) corrections derived from UHF-UCCSDT(Q) calculations may deviate from ROHF-UCCSDT(Q)$_{/B}$ results by as much as 0.26 kcal/mol if the UHF reference suffers from spin contamination, and 0.15 kcal/mol even in the absence of spin contamination. These results underline the importance of specifying the nature of the reference wavefunction and the exact flavor of coupled-cluster methods when discussing open-shell systems.

We have studied the basis set convergence of the HF, CCSD, and (T) contributions to the relative energies using UCCSD(T)-F12b with the AV*n*Z, V*n*Z-F12, and AV*n*Z-F12 basis set, as well as various extrapolations. We propose that Pareto diagrams (Fig. 11) are a useful aid for evaluating the trade-off between basis set size and accuracy. We have found that while VTZ-F12 is very effective at reducing the HF and CCSD basis error found with AVTZ, overall it performs marginally worse than AVTZ due to the upset of error compensation between the HF, CCSD and (T) basis errors. Our results indicate that the additional diffuse functions in the AV*n*Z-F12 family are not required for the accurate description of reactions between polar radicals and polar neutral molecules made of H, C, and O. Considering the efficiency of basis sets, a simple UCCSD(T)-F12b/VQZ-F12 calculation appears to be an excellent

choice, with a peak basis error of 0.08 kcal/mol over the 19 relative energies tested.

Post-(T) corrections up to at least the CCSDT(Q) level appear to be indispensable if one aims to reliably bring the error of classical energies under ±0.5 kcal/mol, as for the moderately multireference TS2 transition state the post-(T) correction reaches −0.9 kcal/mol. It is, therefore, possible that one may gain far more reliability in their energies, by investing their computational budget into CCSDT(Q) calculations instead of chasing the last slivers of basis set error in the valence CCSD(T) correlation energy beyond what CCSD(T)-F12b/VQZ-F12 recovers.

We find that spin–orbit splittings evaluated at the MRCI+Q/AVQZ level appear to be accurate, and there is a partial cessation of SO coupling at the reactant complexes that would not be modeled by simply adding a flat SO contribution to the composite scheme. We propose that the *rotational* ZPE of ·OH can, however, be treated like that.

Our composite benchmark results agree excellently with available ATcT data, and generally also agree with or improve upon previous literature results. We predict a ZPE-inclusive barrier height of 0.55 kcal/mol for $\cdot CH_2OH$ formation and 2.21 kcal/mol for $CH_3O\cdot$ formation. Both of these barrier heights are a point of contention in the literature (Table IV), especially TS2, where barrier heights in the range of 1.2–3.6 kcal/mol have been reported. We expect that pinning down the barrier heights reported in this work with even higher precision would require the consideration of coupled-cluster excitations beyond CCSDT(Q) with an appropriate basis set, calculation of high-accuracy anharmonic vibrational ZPE corrections, the calculation of diagonal Born–Oppenheimer corrections and possibly using a triple zeta basis for CCSDT(Q). Unfortunately, the post-(Q) and large-basis post-(T) calculations will likely require a combination of future advances in hardware and high-order CC implementations to become feasible.

We find that the formation of $CH_2OHO\cdot + H_2$ and $CH_2(OH)_2 + \cdot H$ is thermodynamically favorable, with 0 K reaction enthalpies of −1.72 and −2.43 kcal/mol, respectively. This supports the findings of Ref. 11, where $CH_2OHO\cdot$ and especially $CH_2(OH)_2$ were seen as products in simulations of the ·OH bombardment of $(CH_3OH)_{10}$. It remains to be seen if these product channels become dynamically accessible in bimolecular collisions at higher collision energies, alongside the (possibly water-catalyzed) $\cdot CH_2OH \leftrightarrow CH_3O\cdot$ isomerization and H_2CO formation, but the possibility of rich reaction dynamics taking place is open.

Performing QCT dynamics simulations will of course require the development of a global, full-dimensional potential energy surface, which we hope to publish in future work.

SUPPLEMENTARY MATERIAL

See the supplementary material for all Molpro and MRCC output files (which contain all geometries, energies, and if applicable, harmonic vibrational frequencies) as well as an XLSX spreadsheet containing all energies.

ACKNOWLEDGMENTS

We thank the National Research, Development and Innovation Office–NKFIH, Grant No. K-125317; the Ministry of Human Capacities, Hungary, Grant No. 20391-3/2018/FEKUSTRAT; Project No. TKP2021-NVA-19, provided by the Ministry of Innovation and Technology of Hungary from the National Research, Development and Innovation Fund, financed under the Grant No. TKP2021-NVA funding scheme; and the Momentum (Lendület) Program of the Hungarian Academy of Sciences for financial support. Furthermore, we acknowledge KIFÜ for awarding us access to the computational resource (Budapest2) based in Hungary at Budapest.

AUTHOR DECLARATIONS

Conflict of Interest

The authors have no conflicts to disclose.

Author Contributions

Tibor Győri: Conceptualization (equal); Data curation (lead); Formal analysis (lead); Investigation (lead); Methodology (lead); Visualization (lead); Writing – original draft (lead); Writing – review & editing (equal). **Gábor Czakó**: Conceptualization (equal); Funding acquisition (lead); Project administration (lead); Supervision (lead); Writing – original draft (supporting); Writing – review & editing (equal).

DATA AVAILABILITY

Further data are available from the corresponding authors upon reasonable request.

REFERENCES

[1] E. Herbst, J. Phys. Chem. A **109**, 4017 (2005).
[2] S. E. Cummins, P. Thaddeus, and R. A. Linke, Astrophys. J., Suppl. Ser. **60**, 819 (1986).
[3] K. I. Öberg, S. Bottinelli, J. K. Jørgensen, and E. F. van Dishoeck, Astrophys. J. **716**, 825 (2010).
[4] R. Atkinson, Chem. Rev. **86**, 69 (1986).
[5] C. T. Bowman, Combust. Flame **25**, 343 (1975).
[6] C. K. Westbrook and F. L. Dryer, Combust. Sci. Technol. **20**, 125 (1979).
[7] E. Jiménez, M. K. Gilles, and A. R. Ravishankara, J. Photochem. Photobiol. Chem. **157**, 237 (2003).
[8] J. F. Bott and N. Cohen, Int. J. Chem. Kinet. **23**, 1075 (1991).
[9] K. H. Bates, D. J. Jacob, S. Wang, R. S. Hornbrook, E. C. Apel, M. J. Kim, D. B. Millet, K. C. Wells, X. Chen, J. F. Brewer, E. A. Ray, R. Commane, G. S. Diskin, and S. C. Wofsy, J. Geophys. Res.: Atmos. **126**, e2020JD033439, https://doi.org/10.1029/2020jd033439 (2021).
[10] G. A. Olah, Angew. Chem., Int. Ed. **44**, 2636 (2005).
[11] N. Inostroza-Pino, D. Mardones, J. J. X. Ge, and D. MacLeod-Carey, Astron. Astrophys. **641**, A14 (2020).
[12] L. Pardo, J. R. Banfelder, and R. Osman, J. Am. Chem. Soc. **114**, 2382 (1992).
[13] J. T. Jodkowski, M.-T. Rayez, J.-C. Rayez, T. Bérces, and S. Dóbé, J. Phys. Chem. A **103**, 3750 (1999).
[14] A. Galano, J. R. Alvarez-Idaboy, G. Bravo-Pérez, and M. E. Ruiz-Santoyo, Phys. Chem. Chem. Phys. **4**, 4648 (2002).
[15] S. Xu and M. C. Lin, Proc. Combust. Inst. **31**, 159 (2007).
[16] L. G. Gao, J. Zheng, A. Fernández-Ramos, D. G. Truhlar, and X. Xu, J. Am. Chem. Soc. **140**, 2906 (2018).
[17] O. Roncero, A. Zanchet, and A. Aguado, Phys. Chem. Chem. Phys. **20**, 25951 (2018).
[18] P. del Mazo-Sevillano, A. Aguado, E. Jiménez, Y. V. Suleimanov, and O. Roncero, J. Phys. Chem. Lett. **10**, 1900 (2019).
[19] F. Naumkin, P. del Mazo-Sevillano, A. Aguado, Y. V. Suleimanov, and O. Roncero, ACS Earth Space Chem. **3**, 1158 (2019).

[20]W. Siebrand, Z. Smedarchina, E. Martínez-Núñez, and A. Fernández-Ramos, Phys. Chem. Chem. Phys. **18**, 22712 (2016).
[21]R. A. Jara-Toro, F. J. Hernández, R. A. Taccone, S. I. Lane, and G. A. Pino, Angew. Chem., Int. Ed. **56**, 2166 (2017).
[22]T. L. Nguyen, B. Ruscic, and J. F. Stanton, J. Chem. Phys. **150**, 084105 (2019).
[23]A. J. Ocaña, S. Blázquez, A. Potapov, B. Ballesteros, A. Canosa, M. Antiñolo, L. Vereecken, J. Albaladejo, and E. Jiménez, Phys. Chem. Chem. Phys. **21**, 6942 (2019).
[24]M. A. Ali, M. Balaganesh, F. A. Al-Odail, and K. C. Lin, Sci. Rep. **11**, 12185 (2021).
[25]Y. Benitez, T. L. Nguyen, A. J. Parsons, J. F. Stanton, and R. E. Continetti, J. Phys. Chem. Lett. **13**, 142 (2022).
[26]S. Saebø, L. Radom, and H. F. Schaefer, J. Chem. Phys. **78**, 845 (1983).
[27]E. Henon, F. Bohr, N. Sokolowski-Gomez, and F. Caralp, Phys. Chem. Chem. Phys. **5**, 5431 (2003).
[28]J. D. Watts and J. S. Francisco, J. Chem. Phys. **125**, 104301 (2006).
[29]W. Eisfeld and J. S. Francisco, J. Chem. Phys. **131**, 134313 (2009).
[30]R. J. Buszek, A. Sinha, and J. S. Francisco, J. Am. Chem. Soc. **133**, 2013 (2011).
[31]E. Kamarchik, C. Rodrigo, J. M. Bowman, H. Reisler, and A. I. Krylov, J. Chem. Phys. **136**, 084304 (2012).
[32]C. Barrientos, P. Redondo, H. Martinez, and A. Largo, Astrophys. J. **784**, 132 (2014).
[33]P. Delcroix, M. Pagliai, G. Cardini, D. Bégué, and B. Hanoune, J. Phys. Chem. A **119**, 290 (2014).
[34]P. Kumar, P. Biswas, and B. Bandyopadhyay, Phys. Chem. Chem. Phys. **18**, 27728 (2016).
[35]S. Sarkar, S. Mallick, D. Deepak, P. Kumar, and B. Bandyopadhyay, Phys. Chem. Chem. Phys. **19**, 27848 (2017).
[36]I. Toumi, O. Yazidi, N.-E. Jaidane, M. Al-Mogren, J. Francisco, and M. Hochlaf, J. Chem. Phys. **145**, 244305 (2016).
[37]P. J. Knowles, C. Hampel, and H. J. Werner, J. Chem. Phys. **99**, 5219 (1993).
[38]H.-J. Werner, P. J. Knowles, G. Knizia, F. R. Manby, and M. Schütz, Wiley Interdiscip. Rev.: Comput. Mol. Sci. **2**, 242 (2012).
[39]Molpro, version 2015.1, a package of *ab initio* programs, H.-J. Werner, P. J. Knowles, G. Knizia, F. R. Manby, M. Schütz, P. Celani, W. Györffy, D. Kats, T. Korona, R. Lindh, A. Mitrushenkov, G. Rauhut, K. R. Shamasundar, T. B. Adler, R. D. Amos, S. J. Bennie, A. Bernhardsson, A. Berning, D. L. Cooper, M. J. O. Deegan, A. J. Dobbyn, F. Eckert, E. Goll, C. Hampel, A. Hesselmann, G. Hetzer, T. Hrenar, G. Jansen, C. Köppl, S. J. R. Lee, Y. Liu, A. W. Lloyd, Q. Ma, R. A. Mata, A. J. May, S. J. McNicholas, W. Meyer, T. F. Miller III, M. E. Mura, A. Nicklass, D. P. O'Neill, P. Palmieri, D. Peng, T. Petrenko, K. Pflüger, R. Pitzer, M. Reiher, T. Shiozaki, H. Stoll, A. J. Stone, R. Tarroni, T. Thorsteinsson, M. Wang, and M. Welborn, see https://www.molpro.net.
[40]R. Lindh, U. Ryu, and B. Liu, J. Chem. Phys. **95**, 5889 (1991).
[41]H. J. Werner and P. J. Knowles, J. Chem. Phys. **82**, 5053 (1985).
[42]P. J. Knowles and H.-J. Werner, Chem. Phys. Lett. **115**, 259 (1985).
[43]F. Eckert, P. Pulay, and H.-J. Werner, J. Comput. Chem. **18**, 1473 (1997).
[44]R. D. Amos, J. S. Andrews, N. C. Handy, and P. J. Knowles, Chem. Phys. Lett. **185**, 256 (1991).
[45]P. J. Knowles, J. S. Andrews, R. D. Amos, N. C. Handy, and J. A. Pople, Chem. Phys. Lett. **186**, 130 (1991).
[46]H.-J. Werner, T. B. Adler, and F. R. Manby, J. Chem. Phys. **126**, 164102 (2007).
[47]T. B. Adler, G. Knizia, and H.-J. Werner, J. Chem. Phys. **127**, 221106 (2007).
[48]G. Knizia, T. B. Adler, and H.-J. Werner, J. Chem. Phys. **130**, 054104 (2009).
[49]A. Berning, M. Schweizer, H.-J. Werner, P. J. Knowles, and P. Palmieri, Mol. Phys. **98**, 1823 (2000).
[50]MRCC, a quantum chemical program suite written by M. Kállay, P. R. Nagy, D. Mester, L. Gyevi-Nagy, J. Csóka, P. B. Szabó, Z. Rolik, G. Samu, J. Csontos, B. Hégely, Á. Ganyecz, I. Ladjánszki, L. Szegedy, B. Ladóczki, K. Petrov, M. Farkas, P. D. Mezei, and R. A. Horváth. see www.mrcc.hu.
[51]M. Kállay, P. Nagy, D. Mester, Z. Rolik, G. Samu, J. Csontos, J. Csóka, P. Szabó, L. Gyevi-Nagy, B. Hégely, I. Ladjánszki, L. Szegedy, B. Ladóczki, K. Petrov, M. Farkas, P. Mezei, and Á. Ganyecz, J. Chem. Phys. **152**, 074107 (2020).
[52]Z. Rolik, L. Szegedy, I. Ladjánszki, B. Ladóczki, and M. Kállay, J. Chem. Phys. **139**, 094105 (2013).
[53]M. Kállay and J. Gauss, J. Chem. Phys. **123**, 214105 (2005).
[54]Y. J. Bomble, J. F. Stanton, M. Kállay, and J. Gauss, J. Chem. Phys. **123**, 054101 (2005).
[55]M. Kállay and J. Gauss, J. Chem. Phys. **129**, 144101 (2008).
[56]B. P. Pritchard, D. Altarawy, B. Didier, T. D. Gibson, and T. L. Windus, J. Chem. Inf. Model. **59**, 4814 (2019).
[57]K. L. Schuchardt, B. T. Didier, T. Elsethagen, L. Sun, V. Gurumoorthi, J. Chase, J. Li, and T. L. Windus, J. Chem. Inf. Model. **47**, 1045 (2007).
[58]D. Feller, J. Comput. Chem. **17**, 1571 (1996).
[59]T. Győri and G. Czakó, J. Chem. Phys. **156**, 071101 (2022).
[60]T. H. Dunning, J. Chem. Phys. **90**, 1007 (1989).
[61]R. A. Kendall, T. H. Dunning, and R. J. Harrison, J. Chem. Phys. **96**, 6796 (1992).
[62]M. D. Hanwell, D. E. Curtis, D. C. Lonie, T. Vandermeersch, E. Zurek, and G. R. Hutchison, J. Cheminf. **4**, 17 (2012).
[63]K. A. Peterson and T. H. Dunning, J. Chem. Phys. **117**, 10548 (2002).
[64]C. Hättig, Phys. Chem. Chem. Phys. **7**, 59 (2005).
[65]F. Weigend, Phys. Chem. Chem. Phys. **4**, 4285 (2002).
[66]The aug-cc-pVnZ-JKfit series of auxiliary basis sets are unpublished, but included in the basis set library of Molpro 2015. Molpro defines them as the following: augmented JKfit basis sets were generated from cc-pVnZ-JKfit by adding one even tempered diffuse function to each primitive set. This was done by building $e1^2/e2$ where e1 was the most-diffuse exponent already present and e2 the next most diffuse one if both existed, or e1/2.5 if only one exponent existed beforehand.
[67]K. A. Peterson, M. K. Kesharwani, and J. M. L. Martin, Mol. Phys. **113**, 1551 (2015).
[68]A. Halkier, T. Helgaker, P. Jørgensen, W. Klopper, H. Koch, J. Olsen, and A. K. Wilson, Chem. Phys. Lett. **286**, 243 (1998).
[69]J. M. L. Martin, AIP Conf. Proc. **2040**, 020008 (2018).
[70]K. A. Peterson, T. B. Adler, and H.-J. Werner, J. Chem. Phys. **128**, 084102 (2008).
[71]F. Weigend, A. Köhn, and C. Hättig, J. Chem. Phys. **116**, 3175 (2002).
[72]K. E. Yousaf and K. A. Peterson, J. Chem. Phys. **129**, 184108 (2008).
[73]J. M. L. Martin, Mol. Phys. **112**, 785 (2014).
[74]J. G. Hill, S. Mazumder, and K. A. Peterson, J. Chem. Phys. **132**, 054108 (2010).
[75]D. Peng and K. Hirao, J. Chem. Phys. **130**, 044102 (2009).
[76]W. A. de Jong, R. J. Harrison, and D. A. Dixon, J. Chem. Phys. **114**, 48 (2001).
[77]While the Basis Set Exchange website does not list the aug-cc-pwCVnZ-DK series as available for carbon, it is defined in Molpro as the combination of aug-cc-pwCVnZ and the DK contractions from cc-pVnZ-DK.
[78]S. R. Langhoff and E. R. Davidson, Int. J. Quantum Chem. **8**, 61 (1974).
[79]H.-J. Werner, M. Kállay, and J. Gauss, J. Chem. Phys. **128**, 034305 (2008).
[80]P. J. Knowles and H.-J. Werner, Chem. Phys. Lett. **145**, 514 (1988).
[81]H. J. Werner and P. J. Knowles, J. Chem. Phys. **89**, 5803 (1988).
[82]K. R. Shamasundar, G. Knizia, and H.-J. Werner, J. Chem. Phys. **135**, 054101 (2011).
[83]N. Sylvetsky, M. K. Kesharwani, and J. M. L. Martin, J. Chem. Phys. **147**, 134106 (2017).
[84]J. G. Hill, K. A. Peterson, G. Knizia, and H.-J. Werner, J. Chem. Phys. **131**, 194105 (2009).
[85]B. Brauer, M. K. Kesharwani, S. Kozuch, and J. M. L. Martin, Phys. Chem. Chem. Phys. **18**, 20905 (2016).
[86]W. Kutzelnigg and J. D. Morgan, J. Chem. Phys. **96**, 4484 (1992).
[87]B. Ruscic, R. E. Pinzon, M. L. Morton, G. von Laszevski, S. J. Bittner, S. G. Nijsure, K. A. Amin, M. Minkoff, and A. F. Wagner, J. Phys. Chem. A **108**, 9979 (2004).
[88]B. Ruscic, R. E. Pinzon, G. von Laszewski, D. Kodeboyina, A. Burcat, D. Leahy, D. Montoy, and A. F. Wagner, J. Phys. Conf. Ser. **16**, 561 (2005).
[89]B. Ruscic and D. Bross, Active Thermochemical Tables (ATcT) Thermochemical Values Ver. 1.122r, 2021.

[90]See https://web.archive.org for information about the Internet Archive.
[91]T. J. Lee and P. R. Taylor, Int. J. Quantum Chem. **36**, 199 (1989).
[92]O. Tishchenko, J. Zheng, and D. G. Truhlar, J. Chem. Theory Comput. **4**, 1208 (2008).
[93]CH_3O (g)→CH_2OH (g). https://web.archive.org/web/20220921150527/https://atct.anl.gov/Thermochemical%20Data/version%201.122r/reaction/? & species_number%5B%5D=66 & species_number%5B%5D=79 & c1=-1 & c2=1.
[94]CH_3OH (g) + OH (g) → H (g) + CH_3OOH (g). https://web.archive.org/web/20220727150619/https://atct.anl.gov/Thermochemical%20Data/version%201.122r/reaction/?species_number%5B%5D=16 & species_number%5B%5D=30 & species_number%5B%5D=33 & species_number%5B%5D=102 & c1=1 & c2=-1 & c3=-1 & c4=1.
[95]CH_3OH (g)+OH (g) → H (g) + $CH_2(OH)_2$ (g, conrot gauche). https://web.archive.org/web/20220727152947/https://atct.anl.gov/Thermochemical%20Data/version%201.122r/reaction/?species_number%5B%5D=16 & species_number%5B%5D=30 & species_number%5B%5D=33 & species_number%5B%5D=333 & c1=1 & c2=-1 & c3=-1 & c4=1.
[96]CH_3OH (g) + OH (g) → H (g) + $CH_2(OH)_2$ (g, disrot gauche). https://web.archive.org/web/20220727153211/https://atct.anl.gov/Thermochemical%20Data/version%201.122r/reaction/?species_number%5B%5D=16 & species_number%5B%5D=30 & species_number%5B%5D=33 & species_number%5B%5D=382 & c1=1 & c2=-1 & c3=-1 & c4=1.
[97]CH_3OH (g) + OH (g) → H_2 (g) + H (g) + $CH_2(OO)$ (g). https://web.archive.org/web/20220727154042/https://atct.anl.gov/Thermochemical%20Data/version%201.122r/reaction/?species_number%5B%5D=1 & species_number%5B%5D=16 & species_number%5B%5D=30 & species_number%5B%5D=33 & species_number%5B%5D=510 & c1=1 & c2=1 & c3=-1 & c4=-1 & c5=1.
[98]CH_3OH (g) + OH (g) → CH_3 (g) + H_2O_2 (g). https://web.archive.org/web/20220727154602/https://atct.anl.gov/Thermochemical%20Data/version%201.122r/reaction/?species_number%5B%5D=29 & species_number%5B%5D=30 & species_number%5B%5D=33 & species_number%5B%5D=56 & c1=1 & c2=-1 & c3=-1 & c4=1.
[99]CH_3OH (g) + OH (g) → H_2 (g) + CH_3OO (g). https://web.archive.org/web/20220727155012/https://atct.anl.gov/Thermochemical%20Data/version%201.122r/reaction/?species_number%5B%5D=1 & species_number%5B%5D=30 & species_number%5B%5D=33 & species_number%5B%5D=114 & c1=1 & c2=-1 & c3=-1 & c4=1.
[100]CH_3OH (g) + OH (g) → H_2 (g) + CH_2OOH (g). https://web.archive.org/web/20220727155330/https://atct.anl.gov/Thermochemical%20Data/version%201.122r/reaction/?species_number%5B%5D=1 & species_number%5B%5D=30 & species_number%5B%5D=33 & species_number%5B%5D=806 & c1=1 & c2=-1 & c3=-1 & c4=1.
[101]CH_3OH (g) + OH (g) → CH_4 (g) + HO_2 (g). https://web.archive.org/web/20220727160042/https://atct.anl.gov/Thermochemical%20Data/version%201.122r/reaction/?species_number%5B%5D=20 & species_number%5B%5D=30 & species_number%5B%5D=33 & species_number%5B%5D=53 & c1=1 & c2=-1 & c3=-1 & c4=1.
[102]N. Herrmann and M. Hanrath, J. Chem. Phys. **156**, 054111 (2022).
[103]M. E. Harding, J. Vázquez, B. Ruscic, A. K. Wilson, J. Gauss, and J. F. Stanton, J. Chem. Phys. **128**, 114111 (2008).
[104]CH_3OH (g) + OH (g) → H_2O (g) + CH_2OH (g). https://web.archive.org/web/20220727152509/https://atct.anl.gov/Thermochemical%20Data/version%201.122r/reaction/?species_number%5B%5D=26 & species_number%5B%5D=30 & species_number%5B%5D=33 & species_number%5B%5D=79 & c1=1 & c2=-1 & c3=-1 & c4=1.
[105]CH_3OH (g) + OH (g) → H_2O (g) + CH_3O (g). https://web.archive.org/web/20220727151847/https://atct.anl.gov/Thermochemical%20Data/version%201.122r/reaction/?species_number%5B%5D=26 & species_number%5B%5D=30 & species_number%5B%5D=33 & species_number%5B%5D=66 & c1=1 & c2=-1 & c3=-1 & c4=1.
[106]CH_3OH (g) + OH (g) → H (g) + H_2O (g) + CH_2O (g). https://web.archive.org/web/20220727151032/https:/atct.anl.gov/Thermochemical%20Data/version%201.122r/reaction/?species_number%5B%5D=16 & species_number%5B%5D=26 & species_number%5B%5D=30 & species_number%5B%5D=33 & species_number%5B%5D=36 & c1=1 & c2=1 & c3=-1 & c4=-1 & c5=1.